

CDR Conceptual Design Report of the MPD Cosmic Ray Detector

Authors:

M. Bielewicz^[1,4], L. Swiderski^[1], G. Kasprowicz^[2], P. Kolasinski^[2], D. Wielanek^[2],
M. Rybczyński^[3], E. Jaworska^[1], K. Grodzicki^[1], A. Chłópek^[1,4], I. Shmyrev^[4],
K. Wojcik^[5]

- [1]. National Centre for Nuclear Research, A. Sołtana 7 str., 05-400 Otwock, Świerk, Poland
- [2]. Warsaw University of Technology, Pl. Politechniki 1, 00-661, Warsaw, Poland
- [3]. Jan Kochanowski University, Żeromskiego 5 str., 25-369 Kielce, Poland
- [4]. Joint Institute of Nuclear Research, Joliot-Curie 6 str, Dubna, Russia
- [5]. University of Silesia in Katowice, Bankowa 12 str., 40-007, Katowice, Poland

This page intentionally left blank

Project's Background (MPD)

At JINR Joint Institute for Nuclear Research in Dubna, a project called NICA Nuclotron-based Ion Collider Facility, (NICA is the JINR flagship project for the next decade), is being implemented to create an ionic collider based on the Nuclotron as part of a program to study nuclear matter in a hot and dense state. The main objectives of the program: the creation of an accelerator complex of ions with high luminosity in the collision energy range up to 11 GeV/nucleon for heavy ions and a modern multi-functional detector for the study of heavy ion collisions.

The collider has two crossing points for the beams, which makes it possible to install two detectors and simultaneously carry out two experiments.

One of the detectors, the MPD Multi-Purpose Detector, is planned to study the properties of hot and dense nuclear matter formed during collisions of high-energy heavy ions, in particular, to search for effects associated with deconfinement and/or restoration of chiral symmetry, to study the properties of phase transitions and mixed hadron and quark-gluon phases.

The planned accelerator-accumulative complex will open new great opportunities for carrying out applied programs at JINR in the fields of radiation technology, biology and medicine.

In addition to basic research on the beams of the NICA complex, applied work can also be carried out. JINR has extensive experience in carrying out biomedical research in the field of hadron radiation therapy.

The NICA complex includes various types of accelerators: a linear accelerator, an intermediate energy storage accelerator (booster), the Nuclotron and a collider. These accelerators provide beams in the energy range $E_{\text{lab}} = 1 - 4,5 \text{ A GeV}$ and are required in many applied research programs. The planned accelerator-accumulative complex will open new great opportunities for carrying out applied programs, radiation technologies, biology and medicine at JINR.

As a first step, it was decided to modernize the current accelerator of ions - Nuclotron. The implementation of these ambitious tasks is associated with plans to build the NICA accelerator- complex for ion collisions in a wide range of atomic masses and collision energies (up to $\sqrt{s_{\text{NN}}} = 11 \text{ GeV}$) based on the Nuclotron. The accelerator will have a very high luminosity, $L = 10^{27} \text{ cm}^{-2} \text{ s}^{-1}$. For proton beams, the luminosity should be at the level $L = 10^{31} \text{ cm}^{-2} \text{ s}^{-1}$, and the collision energy is $E_{\text{lab}} = 12,6 \text{ GeV}$.

An important goal of the NICA project is to provide users with a research machine that will allow them to acquire new scientific knowledge, research possibilities and understand the physical properties of a substance at an early stage of its occurrence.

This is an extraordinary set of research tools.

The multi-functional detector MPD is an advanced technical device with many parameters and features that require constant monitoring and control in an on-line mode.

Therefore, the MPD construction requires designing and execution of dedicated technical installations using advanced technologies that will meet the task.

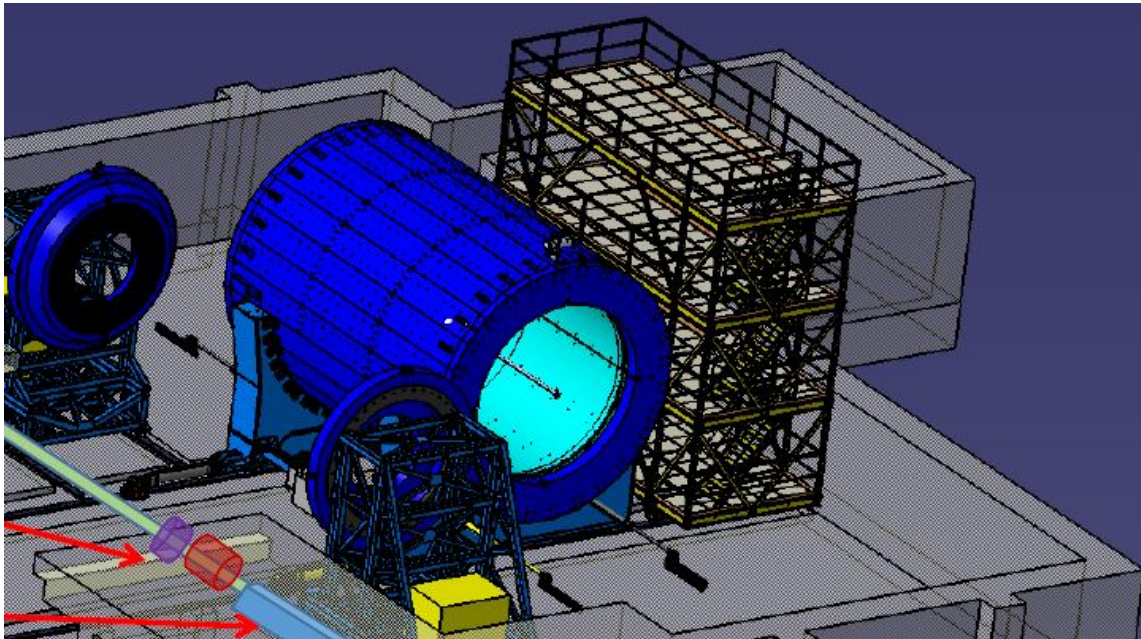


Figure 1 – PLATFORM MPD-NICA andMPD, Mechanical Design.

In Figure 1, the main MPD technical module with the basic infrastructure is shown.

Service requirements for MPD, have led to a design of an integrated structure placed on the wagon, allowing the entire module to be moved within 11 meters for service purposes. Many transmission paths and a high data rate required limit the installation space. Therefore, the MPD control will be placed on a special mechanical structure on four floors. This mechanical block is referred to as the Mechanical Platform. In this design, we will install the MPD infrastructure at 32 RACKs.

1 Contents

This document describes the concept of building a cosmic ray detector for MPD-NICA. The document consists of the following parts:

Chapter 1. (Contents), in addition to the table of contents, includes also the lists of drawings, tables and acronyms.

Chapter 2 (Executive Summary) is a very short summary of why and how we will build this detector.

Chapter 3 (Project Overview) provides an overview of the entire project. The more detailed background of the project and its scope are described. The summary of cost and tentative work schedule is also presented.

Chapter 4 (Project Concept) is the main part of this document. It contains a description of all systems and components being a part of the planned detector. This chapter provides the basic information about the general design of the MCORD along with more detailed description of its mechanical construction and requirements necessary to integrate the MCORD with the MPD. In the next subsections we report a concise description of the muon sensitive scintillation detectors, photodetectors used for light readout, front-end analog electronics and digital signal processing chains and data acquisition system. Information about MCORD capabilities to provide muon based trigger signals is also presented.

Chapter 5 (Evaluation) contains a list of planned test measurements and computer simulations required to design this detector. Evaluation of the MCORD performance is presented, including simulations of cosmic rays reaching the MPD detector, simulations of muons generated during ion-ion collisions and simulations of detector response to recorded particles. The results of laboratory characterization of the detector sections and the procedure for detector commissioning are also given.

In Chapter 6 (References) is a list of references to the literature and materials we refer to in this document.

1.1 Table of Contents

| | |
|--|----|
| Project's Background (MPD) | 3 |
| 1 Contents..... | 5 |
| 1.1 Table of Contents..... | 6 |
| 1.2 Contributors..... | 8 |
| 1.3 Acronyms and Abbreviations..... | 9 |
| 1.4 List of Figures..... | 13 |
| 1.5 List of Tables..... | 15 |
| 2 Executive Summary | 16 |
| 2.1 Introduction | 16 |
| 2.2 Scope..... | 16 |
| 2.3 Cost and Schedule..... | 16 |
| 3 Project Overview | 18 |
| 3.1 Introduction | 18 |
| 3.2 Project Scope..... | 19 |
| 3.3 Cost and Schedule..... | 21 |
| 3.3.1 Cost estimate..... | 21 |
| 3.3.2 Time Schedule | 22 |
| 3.3.3 Gantt chart | 23 |
| 4 Project Concept..... | 25 |
| 4.1 General design..... | 25 |
| 4.1.1 Description..... | 25 |
| 4.1.2 Mechanical Structure..... | 26 |
| 4.1.3 Electrical Structure..... | 29 |
| 4.1.4 Logical Structure..... | 30 |
| 4.2 Scintillators and readout sensors | 32 |
| 4.3 Readout Electronics | 34 |
| 4.4 Digital Electronics (FPGA)..... | 36 |
| 4.5 FPGA Based Muon Trigger | 37 |
| 4.6 Requirements..... | 38 |
| 4.6.1 MCORD integration with MPD..... | 38 |
| 4.6.2 Cable Routes | 39 |
| 4.6.3 User Space in NICA-MPD-PLATFORM | 40 |
| 4.6.4 Power Requirements | 40 |
| 4.6.5 MCORD integration with SCADA WinCC | 41 |

| | | |
|-------|--------------------------------------|----|
| 4.6.6 | DAQ Data Acquisition | 41 |
| 4.6.7 | EqDb Equipment Database..... | 41 |
| 5 | Evaluation..... | 42 |
| 5.1 | Cosmic Shower Simulations | 42 |
| 5.2 | MPD subsystems calibration..... | 46 |
| 5.3 | Detector Response Simulations..... | 54 |
| 5.4 | Detector Performance Evaluation..... | 56 |
| 6 | References | 60 |

1.2 Contributors

M. Bielewicz^[1,5,*], A. Bancer^[1], M. Barabanov^[5], A. Chlopik^[1,5], M. Czarnynoga^[2,5], D. Dabrowski^[2,5], A. Dudzinski^[1], M. Grodzicka-Kobylka^[1], J. Grzyb^[1], K. Grodzicki^[1], E. Jaworska^[1], P. Kankiewicz^[3], G. Kasproicz^[2], A. Kisiel^[2,5], P. Kolasinski^[2], S. Kowalski^[6], M. Kuich^[4], J. Lukasik^[7], B. Maksiak^[1], J. Marzec^[2], T. Matulewicz^[4], S. Mianowski^[1], M. Milewicz-Zalewska^[2,5], M. J. Peryt^[2,5], A. Pollo^[1], K. Pozniak^[2], F. Protoklitow^[2,5], D. Pszczel^[1], S. Pulawski^[6], R. Romaniuk^[2], K. Roslon^[2,5], M. Rybczynski^[3], J. Rzadkiewicz^[1], I. Shmyrev^[5], G. Stefanek^[3], J. Stepaniak^[1], E. Strugalska-Gola^[1], L. Swiderski^[1], T. Szczesniak^[1], M. Szuta^[1], A. Syntfeld-Kazuch^[1], A. Vodopyanov^[5], D. Wielanek^[2], Z. Wlodarczyk^[3], K. Wojcik^[6], W. Zabolotny^[2]

[1]. National Centre for Nuclear Research, A. Sołtana 7 str., 05-400, Otwock-Świerk, Poland

[2]. Warsaw University of Technology, Pl. Politechniki 1, 00-661, Warsaw, Poland

[3]. Jan Kochanowski University, Żeromskiego 5 str., 25-369 Kielce, Poland

[4]. Warsaw University, Krakowskie Przedmieście 26/28 str., 00-927, Warsaw, Poland

[5]. Joint Institute of Nuclear Research, Joliot-Curie 6 str., 141980, Dubna, Russia

[6]. University of Silesia in Katowice, Bankowa 12 str., 40-007, Katowice, Poland

[7]. Institute of Nuclear Physics PAN, Radzikowskiego 152 str., 31-342, Krakow, Poland

* Corresponding Author: Marcin.Bielewicz@ncbj.gov.pl

1.3 Acronyms and Abbreviations

Table 1 – Acronyms and Abbreviations.

| <i>Acronyms and Abbreviations</i> | | |
|-----------------------------------|---------|--|
| 1. | (H) | Horizontal Measurement |
| 2. | (V) | Vertical Measurement |
| 3. | A | Ampere |
| 4. | Å | Angstrom |
| 5. | AC | Alternating Current |
| 6. | ACS | Access Control System |
| 7. | ADC | Analog to Digital Converter |
| 8. | ADT | Array Display Tool |
| 9. | ANSI | American National Standards Institute |
| 10. | APPS | Accelerator Personnel Protection System |
| 11. | ASIC | Application-Specific Integrated Circuit |
| 12. | ASME | American Society of Mechanical Engineers |
| 13. | ASTM | American Society for Testing and Materials |
| 14. | AWG | American Wire Gauge |
| 15. | BAG | Bayard-Alpert Gauge |
| 16. | BBA | Beam Based Alignment |
| 17. | BCJINR | Building Code of JINR |
| 18. | BDA | Beam Defining Aperture |
| 19. | BLM | Beam Loss Monitor |
| 20. | BM | Bending Magnet |
| 21. | BPM | Beam Position Monitor |
| 22. | B-SR | Booster-to-Storage Ring |
| 23. | BT | Beamline Team |
| 24. | CA | Channel Access |
| 25. | CAD | Computer Aided Design |
| 26. | CAMAC | Computer Automated Measurement And Control |
| 27. | CCAS | Cable Connection Authorization System |
| 28. | CCG | Cold Cathode Gauge |
| 29. | CCTV | Closed Circuit TeleVision |
| 30. | CDR | Conceptual Design Report |
| 31. | CPU | Central Processing Unit |
| 32. | c-RIO | Compact RIO |
| 33. | CRWS | Cable Race Way System |
| 34. | DAC | Digital to Analog Converter |
| 35. | DC | Direct Current |
| 36. | DIAMOND | British National Synchrotron |
| 37. | DMM | Digital Multi Meters |
| 38. | DP | Display Page |
| 39. | DSP | Digital Signal Processor |
| 40. | ECS | Experiment Control System |
| 41. | EqDb | Equipment Database |
| 42. | ESD | Emergency Shutdown |
| 43. | ESH | Environmental Safety and Health |
| 44. | ESRF | European Synchrotron Radiation Facility |
| 45. | EUV | Extreme Ultraviolet |
| 46. | FAS | Fire Alarm System |
| 47. | FFT | Fast Fourier Transform |
| 48. | FPGA | Field Programmable Gate Array |
| 49. | FTIR | Fourier Transform InfraRed |
| 50. | GbE | Gigabit Ethernet |
| 51. | GHe | Gaseous Helium |
| 52. | GPIO | General Purpose Interface Bus |

| | | |
|------|-----------------|--|
| 53. | GSS | Gas Supply System |
| 54. | GUI | Graphical User Interface |
| 55. | GV | Gas Valve |
| 56. | Gy | Gray, a unit for measuring radiation dose |
| 57. | H | Henry, a measure of inductance |
| 58. | HMI | Human Interface |
| 59. | HP | High Pressure, high purity, horse power |
| 60. | HPS | Hazardous Production Material |
| 61. | HQS | High Quality Service |
| 62. | HTSC | High Temperature Superconductor |
| 63. | HVAC | Heating Ventilating and Air Conditioning |
| 64. | IOC | Input Output Controller |
| 65. | IOT | Inductive Output Tube |
| 66. | IPD | Intelligent Power Distributor |
| 67. | ISO | International Organization for Standardization |
| 68. | IT | Information Technology |
| 69. | LEED | Leadership in Energy and Environmental Design |
| 70. | LHe | Liquid Helium |
| 71. | LID | Long Insertion Device |
| 72. | LinAc | Linear Accelerator |
| 73. | LLRF | Low Level Radio Frequency |
| 74. | LN ₂ | Liquid Nitrogen |
| 75. | LOI | Letters of Intent |
| 76. | LPG | Low Pressure Gas |
| 77. | LTS | Low Temperature Superconductor |
| 78. | M | meter, or mill, if a Prefix |
| 79. | M | Million, or Mega |
| 80. | mA | miliAmper 10 ⁻³ A |
| 81. | MCL | Multichannel Line |
| 82. | MPD | Multi-Purpose Detector |
| 83. | MRAM | Magnetic Random-Access Memory |
| 84. | n | Nano, 1 x 10 ⁻⁹ |
| 85. | nC | Nano Coulomb (Measure of Electrical Charge) |
| 86. | NFPA | National Fire Protection Administration |
| 87. | NICA | Nuclotron-based Ion Collider fAcility |
| 88. | ODH | Oxygen Deficiency Hazard |
| 89. | OPI | Operator Interface |
| 90. | ОИЯИ | Объединенный институт ядерных исследований |
| 91. | ph/s | photons per second |
| 92. | PID | Proportional Integral Derivative |
| 93. | PLC | Programmable Logic Controller |
| 94. | PLS | Power Line Switch |
| 95. | PM | Permanent Magnet |
| 96. | PMS | Position Monitoring System |
| 97. | PPM | Pure Permanent Magnet |
| 98. | PPMS | Physical Properties Measurement System |
| 99. | PPS | Personnel Protection System |
| 100. | PRF | Pulse Repetition Frequency |
| 101. | ps | picosecond |
| 102. | psf | pounds per sqft |
| 103. | rad | radian |
| 104. | RF | Radio Frequency |
| 105. | RFI | Radio Frequency Interference |
| 106. | RGA | Residual Gas Analyzer |
| 107. | RS-232 | Recommended Standard 232 (serial interface) |
| 108. | RS-485 | Recommended Standard 485 (serial interface) |
| 109. | RTOS | Real-Time Operating System |
| 110. | SAS | Sound Alert System |

| | | |
|------|------------------|--|
| 111. | SCADA | Supervisory Control And Data Acquisition |
| 112. | SCS | Slow Control System |
| 113. | SNR | Signal-to-Noise Ratio |
| 114. | SPring-8 | Japanese National Synchrotron |
| 115. | STS | Suggested Technical Solution |
| 116. | TC | ThermoCouples |
| 117. | THz | TerraHertz |
| 118. | UBPM | User Beam Position Monitors |
| 119. | UHR | Ultra-High Resolution |
| 120. | UHV | Ultra-High Vacuum |
| 121. | UPS | Uninterruptible Power Supply |
| 122. | USB | Universal Serial Bus |
| 123. | UV | Ultraviolet |
| 124. | VLS | Variable Line Spacing |
| 125. | VME or VMEbus | Versa Module Europa bus |
| 126. | VUV | Vacuum Ultraviolet |

Table 2 – Add Acronyms and Abbreviations.

| <i>Acronyms and Abbreviations</i> | | |
|-----------------------------------|-----------|---|
| 127. | ACORDE | ALICE Cosmic Ray DEtector |
| 128. | AFE | Analog Front End |
| 129. | ALICE | ALargeIon Collider Experiment |
| 130. | AMC | Advanced Mezzanine Card |
| 131. | ASCII | American Standard Code for Information Interchanged |
| 132. | CAN | Controller Area Network |
| 133. | CERN | Conseil Européenne pour la Recherche Nucléaire |
| 134. | CMS | Compact Muon Solenoid |
| 135. | CoREAS | Corsika based Radio Emission from Air Showers |
| 136. | CORSIKA | COsmic Ray Simulations for KAscade |
| 137. | CRT | Coincidence Resolving Time |
| 138. | DAQ | Data Acquisition |
| 139. | DCS | Detector Control System |
| 140. | FMC | FPGA Mezzanine Card |
| 141. | GEANT4 | Toolkit for Simulation of the Passage of Particles through matter |
| 142. | GSI | Helmholtz Zentrum für Schwerionenforschung |
| 143. | HDL | Hardware Description Language |
| 144. | HEP | High Energy Physics |
| 145. | IPMI | Intelligent Platform Management Interface |
| 146. | JINR | Joint Institute for Nuclear Research |
| 147. | LDO | Low Drop Out |
| 148. | MCA | Micro Channel Architecture |
| 149. | MCH | MTCA Carrier Hub |
| 150. | MCNPX | Monte Carlo N Particle Transport Code |
| 151. | MCORD | MPD COsmic Ray Detector |
| 152. | MPPC | Multi Pixel Photon Counters = SiPM |
| 153. | MTCA | Micro TCA standart |
| 154. | PMT | Photon Multiplier Tube |
| 155. | PoE | Power over Ethernet |
| 156. | RF | Radio Frequency |
| 157. | RTM | Rear Transition Module |
| 158. | SHOWERSIM | A Modular Monte Carlo software system for Air Shower simulations |
| 159. | SiPM | Silicon Photo Multipliers |
| 160. | TCA | Telecom Computing Architecture |
| 161. | TDC | Time to Digital Converter |

| | | |
|------|-----|-------------------------|
| 162. | TDR | Technical Design Report |
| 163. | TOF | Time of Flight |
| 164. | TPC | Time Projector Chamber |
| 165. | WAN | Wide Area Network |

1.4 List of Figures

| | |
|--|-----------|
| Figure 1 – PLATFORM MPD-NICA andMPD, Mechanical Design..... | 4 |
| Figure 2 – The NICA complex [1]..... | 18 |
| Figure 3 – MPD detectors and Platform for MPD electronics racks [2]..... | 18 |
| Figure 4 – Conceptual design of the MCORD detector. | 19 |
| Figure 5 – One MCORD section with electronic components. | 20 |
| Figure 6 – The MCORD project Gantt chart..... | 23 |
| Figure 7 – MCORD idea scheme. | 25 |
| Figure 8 – Basic functional element of the MCORD:Section with electronic. | 26 |
| Figure 9 – The MCORD structure (in red color) on MPD surface. | 27 |
| Figure 10 – Installation of MCORD modules on MPD surface. | 27 |
| Figure 11 – The central section is above the two others. | 27 |
| Figure 12 – Screws on the angle bars connecting the MPD drum to the legs. | 28 |
| Figure 13 – MCORD module frame for the upper part of the MPD barrel..... | 28 |
| Figure 14 – MCORD module frame for the lower part of the MPD barrel..... | 28 |
| Figure 15 – System architecture based on MTCA standard. | 29 |
| Figure 16 – Logic diagram of the MCORD detector. | 31 |
| Figure 17 – Scintillator inside an aluminum cover. | 32 |
| Figure 18 – Cross-sections of single detector with aluminum cover. | 32 |
| Figure 19 – Scintillator assembled into a section comprising 8 detectors. | 33 |
| Figure 20 – MCORD muon detection module..... | 33 |
| Figure 21 – MCORD installed around the MPD. | 33 |
| <i>Figure 22 – Basic functionality of the AFE module.....</i> | <i>34</i> |
| Figure 23 – Basic functionality of the HUB module. | 35 |
| Figure 24 – Dataflow on FMC and AMC boards. | 36 |
| Figure 25 – Architecture of MTCA crate, ver. 4. | 37 |
| Figure 26 – MCORD module, HUB and cables system on the MPD surface..... | 39 |
| Figure 27 – MCORD module, HUB and cables system on the MPD surfacever.2. . | 39 |
| Figure 28 – Cable routes from the MCORD to the NICA-MPD-PLATFORM. | 40 |
| Figure 29 – Angular distributions of Extensive Air Shower components..... | 43 |
| Figure 30 – Average number of muons per one primary particle. | 44 |
| Figure 31 – Angular distribution of muons from EAS..... | 44 |
| <i>Figure 32 – To study the propagation of cosmic rays in the MPD detector.</i> | <i>45</i> |
| Figure 33 – Energy dependence of muon transmission coefficient. | 45 |
| <i>Figure 34 – Normalized distribution of the effective angle of muons rescattering. .</i> | <i>46</i> |

| | |
|---|-----------|
| <i>Figure 35 – Cosmic muon flux as a function of incident muon zenith angle.....</i> | <i>47</i> |
| <i>Figure 36 – Momentum integral spectrum of cosmic muons.</i> | <i>47</i> |
| <i>Figure 37 – MCORD sections numbering and visualization of the full setup.</i> | <i>48</i> |
| <i>Figure 38 – TPC visualization inside the MPD.</i> | <i>48</i> |
| <i>Figure 39 – ToF detectors numbering inside the MPD.</i> | <i>49</i> |
| <i>Figure 40 – Plot of all hit positions of the analyzed detector setup.</i> | <i>49</i> |
| <i>Figure 41 – Coincidence of selected MCORD modules.</i> | <i>50</i> |
| <i>Figure 42 – MCORD configurations A, B and C for TPC calibration.</i> | <i>50</i> |
| <i>Figure 43 – Distribution of track lengths for coincidence events.....</i> | <i>51</i> |
| <i>Figure 44 – MCORD configurations D and E for TPC calibration.</i> | <i>51</i> |
| <i>Figure 45 – Distribution of track lengths for coincidence events.....</i> | <i>52</i> |
| <i>Figure 46 – MCORD (outer ring) and ToF (inner ring) MPD sections numbering.</i> | <i>53</i> |
| <i>Figure 47 – Muons and pions distribution inside the MPD.....</i> | <i>55</i> |
| <i>Figure 48 – The points of creation of negative and positive muons.</i> | <i>56</i> |
| <i>Figure 49 – The energy spectra of dark counts.....</i> | <i>57</i> |
| <i>Figure 50 – The experimental setup for measuring the coincidence.....</i> | <i>57</i> |
| <i>Figure 51 – The muons energy spectra.....</i> | <i>58</i> |
| <i>Figure 52 – Timing spectra recorded for muons.....</i> | <i>58</i> |
| <i>Figure 53 – The relation between the CRT time and the distance.....</i> | <i>59</i> |

1.5 List of Tables

| | |
|---|-----------|
| Table 1 – Acronyms and Abbreviations. | 9 |
| Table 2 – Add Acronyms and Abbreviations. | 11 |
| Table 3 –The main components of the system and estimated costs of implementing the MCORD Project. | 21 |
| <i>Table 4 – Effective rescattering angle for muons with different Energy thresholds passing the MPD.</i> | <i>46</i> |
| Table 5 – Number of counts per hour for coincidence events detected by two MCORD modules and TPC calculated for muons with momentum $p > 1.6 \text{ GeV}/c$ | 50 |
| Table 6 – Number of counts per hour for coincidence events detected by two MCORD modules and TPC calculated for muons with momentum $p > 1.6 \text{ GeV}/c$ | 52 |
| Table 7 – Number of counts per hour for coincidence events detected by two MCORD modules and ToF or two MCORD modules and ToF and TPC calculated for muons with momentum $p > 0.1 \text{ GeV}/c$ | 53 |
| Table 8 – Number of counts per hour for coincidence events detected by two MCORD modules and ToF or two MCORD modules and ToF and TPC calculated for muons with momentum $p > 1.6 \text{ GeV}/c$ | 54 |
| Table 9 – Number of counts per hour for coincidence events detected by two MCORD modules and ToF or two MCORD modules and ToF and TPC calculated for muons with momentum $p > 10 \text{ GeV}/c$ | 54 |

2 Executive Summary

The detector is proposed by a Polish consortium NICA-PL comprising several Polish scientific institutions. The goals and basic assumptions for the MCORD were defined by the MCORD team. The MCORD team is open to new collaborators to participate in the preparation of the project.

2.1 Introduction

This report presents a concept of constructing a detector dedicated for detection of muons observed during measurements carried out at the MPD detector that is currently under construction at the NICA facility. The MPD detector is not equipped with a dedicated muon detector. It has been proposed to design and build an additional detector that will complement the current MPD set and increase its measurement capabilities. The main goal of this project is to provide information from cosmic muons that pass the MPD detector in both in-beam and off-beam experiments. Hence, the detector is called the MPD Cosmic Ray Detector (MCORD).

The data from cosmic ray muons could be used as a trigger for calibration of other detection systems comprising the MPD detector. Large surface covered by the MCORD offers also possibility for efficient registration of muons generated in expanding atmospheric showers induced by distant sources. Moreover, beyond some energy threshold, observation of muons originating from decays of collision products will also be possible. In this report examples of the MCORD functionality as a part of the MPD detector are presented.

2.2 Scope

The MCORD is designed as a universal, fast triggering system built as a modular reconfigurable construction. The detection system will be based on plastic scintillators equipped with optical fibers, and semiconductor photomultipliers (SiPM) will be used to read the light. Thanks to this solution, good quality and fast measurements will be combined with the relatively small price of this potentially large detector. The analysis of received signals will take place using the digital FPGA modules, which will ensure full flexibility in expanding the tasks that the system will have to fulfill. Due to the modular design, the same system (its small part) will be able to be used for both laboratory testing of other MPD sub-detectors, and the calibration of these detectors after placing them inside the MPD in off-beam mode. The full detector will support these systems as an additional trigger, calibrator, and muon identifier during the normal operation of the MPD detector with the beam. Thanks to its unique construction, it will expand the possibilities of collecting scientific data of the MPD detector with astrophysical observations.

2.3 Cost and Schedule

The preparation of the detector concept and the design along with the construction of the demonstrator should take up to 2-3 years. The demonstrator will consist of the two basic MCORD detector units (section) with full signal control, reception and analysis functionality. The demonstrator will be used for both the system testing and the evaluation as well as for the first laboratory tests of other sub-detectors. Construction of the full detector will take place successively in the next approximately 2 years. Due to the modular

construction, it is not required to build a full detector to start working. Further the MCORD detector modules will be added successively along with their construction.

The cost of materials for the construction of a single MCORD detector section, when building the entire detector, is less than USD 20,000. The full MCORD detector will consist of 28 modules, each module with three sections. Thus, the cost of building the entire detector will be approximately USD 1,500,000. The cost of building the first sections for the demonstrator will be higher and will be approximately US \$ 30,000. The labor costs must also be added to the costs described above.

3 Project Overview

3.1 Introduction

A new accelerator complex was designed at the Joint Institute for Nuclear Research (JINR) in Dubna to study properties of dense baryonic matter. One of the main parts of the Nuclotron-based Ion Collider fAcility (NICA, see Figure 2) [1] is the Multi-Purpose Detector (MPD) [2]. The MPD is placed in a dedicated experimental hall and its operation is managed by a Slow Control System [3], [4] installed in racks located on a NICA-MPD-PLATFORM [5] placed by the MPD (Figure 3). The MPD detector was designed to track products emitted during ion-ion collisions that will take place in one of two crossing points of beams accelerated in opposite directions. The role of the MPD is to provide information necessary for reconstructing each event. However, so far it has not been considered to trace muons passing through the MPD detector. There are two sources of muons that could provide valuable data. One of them is muons born in atmosphere due to collisions of charged particles arriving to Earth from outer space, henceforth referred to as “cosmic muons”. The second one is secondary muons produced from decays of products of beam-beam collisions. MPD is not equipped with a dedicated muon detector.

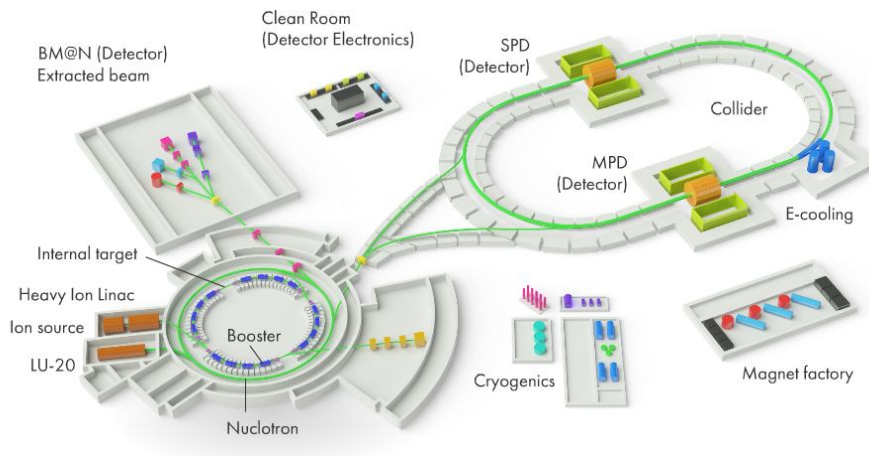


Figure 2 – The NICA complex [1].

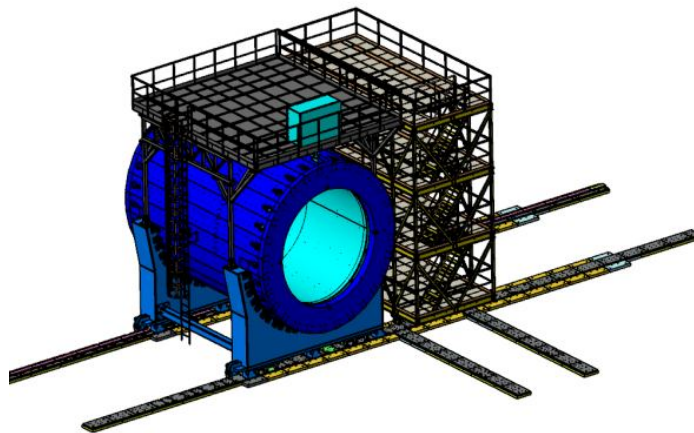


Figure 3 – MPD detectors and Platform for MPD electronics racks [2].

Cosmic muons are one of the background sources in high energy physics experiments [6] as they generate similar or even identical signals as charged particles produced during collisions or during decays of neutral products. Therefore, the MPD needs an additional triggering system that could be used to recognize some of muons produced during collisions and to discriminate signals induced by cosmic muon showers. Secondly, since cosmic muons background provides stable flux of muons passing the MPD independently from beam experiments, a muon detection system could also be used for off-beam calibration of the MPD response to muons. Muon induced signals can also provide the opportunity to test the triggering efficiency of different MPD subsystems, the Experiment Control Systems (ECS) and finally, the Data Acquisition (DAQ).

Moreover, the information about high energy muon showers could also be collected during almost all time of the MPD operation, even off-beam. This would be valuable source of data for astrophysics experiments, enabling reconstruction of source location on the hemisphere.

3.2 Project Scope

In order to enrich the MPD with these features, we propose to surround the MPD with a cosmic-ray detector called MCORD (Figure 4) [7], [8]. A similar system was constructed at CERN for the ALICE detector (ACORDE [9]). The main difference is that ALICE was located deep underground, whereas the MPD is located on ground level. The specific location of ALICE and ACORDE forms a natural barrier that filters low energy muons and most of other charged particles and gamma rays. Moreover, detected muons come only from the zenith direction. The MPD with the MCORD will be located on ground level, therefore it will detect muons coming from all directions between the zenith and the horizon, filtered and suppressed to some extent only by concrete walls of the experimental hall.

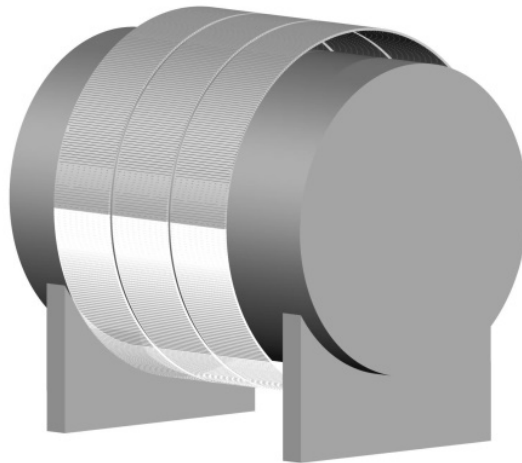


Figure 4 – Conceptual design of the MCORD detector.

Preliminary discussions between partners involved in the project point to plastic scintillators with light readout as most suitable candidates for a detector module. In the initial stage of the project experiments and simulations were done to choose the optimum shape of scintillators, the configuration of photo-detectors and readout electronics. The most commonly used material for muon detection is plastic scintillator, relatively cheap and efficient, an advantage in case of large size installations like the MPD. Plastics with wavelength shifting (WLS) fibers are proposed to detect muons around the MPD. As

scintillation readout, we propose using silicon photomultipliers (SiPMs) [10], installed at both ends of each scintillator, taking advantage of their small size, robustness and insensitivity to magnetic field. Detector modules will be arranged in a barrel shape around the central part of the MPD detector (Figure 4). In the second phase of the project, two detector sections comprising 16 plastic bars (MCORD demonstrator) will be provided for calibration and testing other sub-detectors system before and after their assembling inside of the MPD. In the third stage we propose to build 2 to 6 module comprising 24 scintillating bars each that could be used for off-beam MPD subsystems calibration in service position. The final stage of the project involves the construction of the full-size MCORD detector, as well as its installation, commissioning and integration on the MPD.

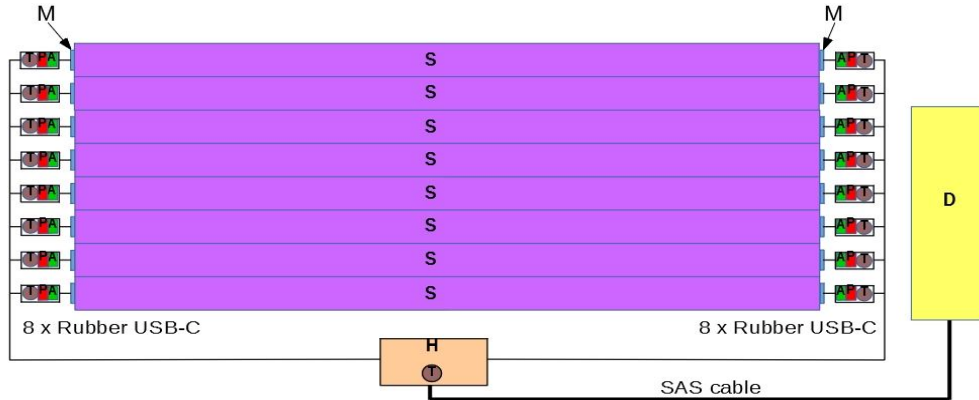


Figure 5 – One MCORD section with electronic components.

Legend: S violet – scintillator, M blue – SiPM, R red – power supply, T brown – temperature sensor, A green – amplifier, (R and T and A) – The Analog Front End Electronic(AFE), H orange – Hub & Power Splitter, D yellow – MicroTCA system

The main assumption made during design stage of the MCORD detector was its modular construction. The detector will be divided into modules and these will be divided into smaller sections. Each of these elements will be separated from the rest and can work as an independent detector. Thanks to this solution, it will be possible to use the MCORD detector parts for testing and calibration of other sub-detectors regardless of their size. The MCORD detector will be composed of 28 modules, and it will comprise over six hundreds of double-side readout detectors. One MCORD module consists of three sections and a support frame, with central section slightly elevated above the first one and the third one. Each section consists of eight scintillators with analog and digital electronic system (see Figure 5). Each SiPM detector will be directly connected to its own Analog Front-End module (AFE) located inside the end part of scintillator aluminum cover. The AFE consists of an amplifier, power supply and temperature compensation circuit. The second part of the analog readout electronic is a passive HUB module. The main functionality of the HUB is, to control the power delivery to the AFE boards and to distribute analog signals from AFE to the digital electronic. The analog signal from the SiPM is send by the passive HUB to the ADC module. The ADC digitizes the signals and sends them to an FPGA chip. The signal analyze system (based on FPGA electronic) is a part of MicroTCA (MTCA) crate (MicroTCA® is a modular, open standard for building high performance switched fabric computer systems in a small form factor [11]). One MTCA crate receives signals from up to 384 channels (SiPMs). Data from the MTCA can be finally passed to a PC over the Ethernet connection.

MCORD should be able to provide information about the time and amplitude of the signals at both ends of scintillators. The position of the hit along the scintillator will be calculated from the time difference between those signals. The track and direction of the

muon will be calculated in the FPGA based on coincident hits from different detector layers. Based on these data, testing and calibration of the TPC [12] (Time Projection Chamber) detector and the TOF [13] (Time of Flight) detectors should be possible. Since MCORD will cover a substantial fraction of the MPD volume, it could also be very useful for observations of cosmic showers initiated by extremely high energy primary particles coming from the horizon direction.

3.3 Cost and Schedule

3.3.1 Cost estimate

The cost of building the MCORD detector can be divided into several categories: material and equipment purchase, labor costs (design, simulations, construction, testing), transport and administrative costs. Table 3 shows an approximate calculation of all material and equipment costs necessary to build 28 MCORD detector modules along with all electronics servicing and analyzing physical data. The initial work and construction of the demonstrator was done by the MCORD team based on grants received for this purpose. The labor costs of team members will be partly supported with funds obtained in Poland. Most of the costs of materials needed to build a full detector (without the costs of building a demonstrator) should be obtained from the NICA project.

To sum up, in order to get the estimated full construction cost of the MCORD detector, the total amount shown in Table 3 should add labor costs of approximately USD 1 million (to be spent in a period about 4 years). Assuming a reserve fund for additional unexpected expenses of USD 300,000, the total cost of the project will not exceed USD 3 million.

Table 3 –The main components of the system and estimated costs of implementing the MCORD Project.

| | Description | USD |
|-----|--------------------|----------------------|
| 1. | Scintillators | 667 296 USD |
| 2. | SiPM sensors | 172 200 USD |
| 3. | Aluminum profiles | 9 408 USD |
| 4. | AFE modules | 141 120 USD |
| 5. | USB-C cables | 83 700 USD |
| 6. | Passive HUB | 55 568 USD |
| 7. | SAS cables | 55 568 USD |
| 8. | SMA cables | 93 450 USD |
| 9. | FMC-TDC carts | 79 976 USD |
| 10. | AMC-FMC carts | 113 360 USD |
| 11. | MTCA crate | 49 052 USD |
| 12. | PoE switch | 3 845 USD |
| 13. | Module frames | 210 000 USD |
| 14. | TOTAL | 1 687 475 USD |

3.3.2 Time Schedule

Conceptual work on the MCORD project began in 2018. As part of this work, the first detector concepts and documentation were prepared. In 2019-2020, JINR grants were obtained, allowing for procurement of materials and equipment necessary to perform initial tests and for constructing 2 sections demonstrating muon detection. The demonstrator will consist of two sections (eight scintillators each) along with the electronics that controls and analyze data. After laboratory characterization, ready-to-use demonstrator will be delivered to Dubna in the end of 2020. Subsequently, it is planned to provide two full modules (3 sections each) to the end of 2021. Our team will apply for additional funding to build 6 MCORD modules by the end of 2021. The number here will significantly increase the efficiency of using MCORD for initial testing and calibration of other MPD detectors. The schedule of further work on construction the full MCORD, will depend on the date of obtaining funds for further construction.

It is proposed to divide the MCORD project into 4 stages (see Gantt chart in the chapter 3.3.3) devoted to:

- Stage 1: Concept and Design;
- Stage 2: Prototype production;
- Stage 3: The first 2-6 MCORD module production, including installation and commissioning at MPD;
- Stage 4: Operation work and MCORD extension to full 28 modules.

Stage 1: Create a collaboration group of scientists and engineers. Design will focus on the choice of most appropriate and cost efficient detector comprising plastic scintillators, photo-detector, front-end and readout electronics. It is planned that stage one will last about 18-21 months.

Stage 2 Characterization of the optimized scintillator detector module with SiPMs coupled at both ends and readout with optimized electronics developed for the MCORD. Following the characterization of base parameters concerning muon detection, the MCORD demonstrator (2 sections – 16 scintillators) will be constructed and tested in laboratory conditions. As a next step, these sections will be shipped to the NICA facility in Dubna and will be used to test and calibrate MPD sub-detectors in laboratory conditions. It is planned that stage 2 one will take about 21 months.

Stage 3: Production of 2 to 6 full-scale MCORD modules (3 sections each) that can be used for more advanced laboratory tests. The modules can be also placed on the surface of the MPD detector. The modules will be fully operational to provide the first data with cosmic muons and serve as a trigger for calibration of other MPD sub-detectors (TPC, TOF, eCal). It is planned that stage 3 will take about 18 months.

Stage 4: In this phase of our work, the MCORD team will start the normal operational maintenance of the detector (data collection and calibration of other sub-detectors using 2-6 modules). At the same time, as funds are obtained, the construction of further MCORD modules will continue. It is anticipated that the MCORD detector will be extended by two modules every quarter on average.

3.3.3 Gantt chart

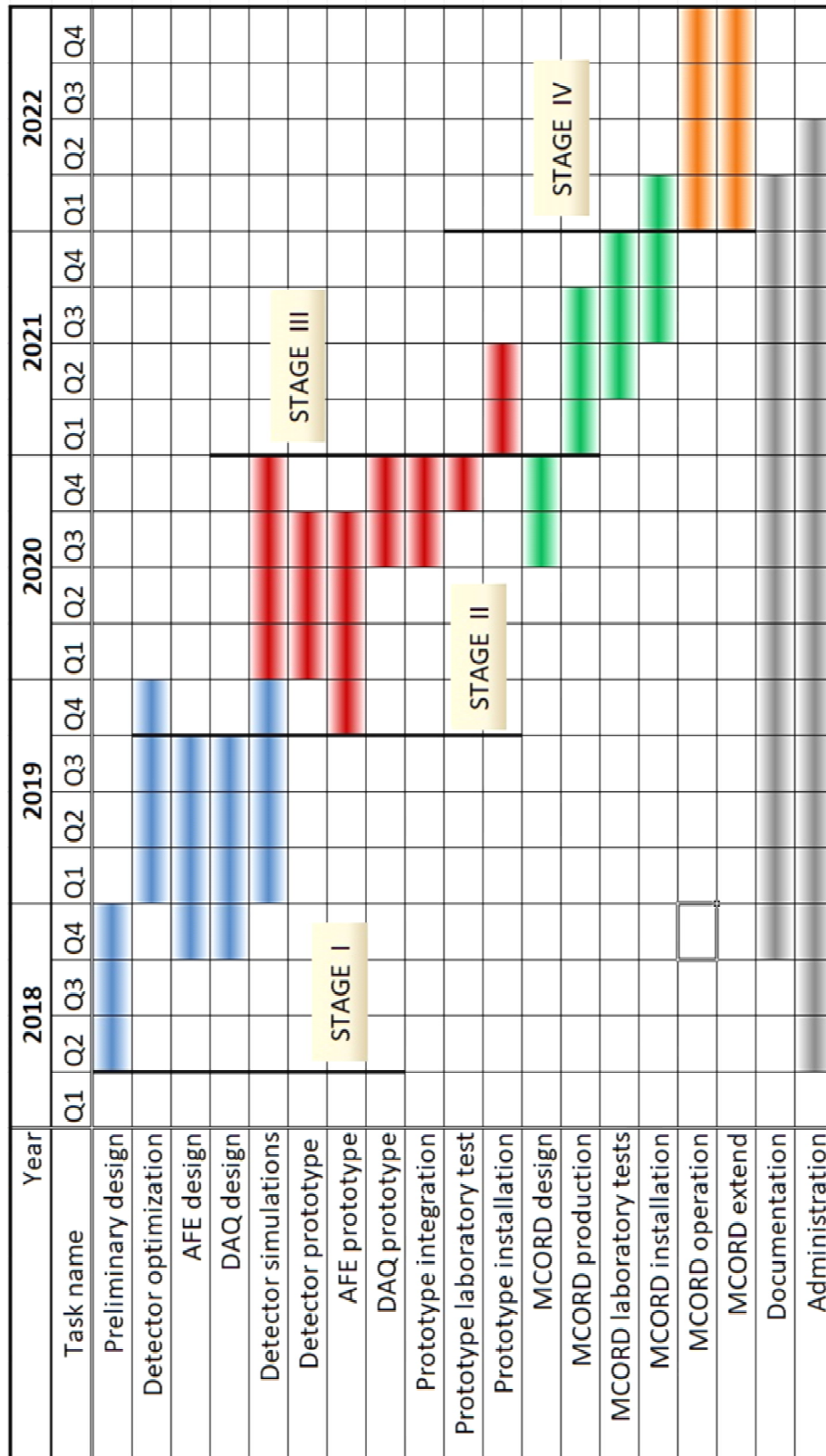


Figure 6 – The MCORD project Gantt chart

This page intentionally left blank

4 Project Concept

4.1 General design

4.1.1 Description

The MCORD detector will be composed of plastic scintillator bars with wavelength shifting (WLS) fibers for light collection and transport to readout devices installed at both ends of plastic bars (Figure 7). For light readout, silicon photomultipliers (SiPM, also known as multi-pixel photon counters – MPPCs) will be used. Their small size is an advantage over traditional PMTs as it helps to provide high level of coverage. Since the MPD detector comprises a large magnet around which the MCORD detector should be installed, the use of SiPM photodetectors is also beneficial, as they are insensitive to the magnetic field.

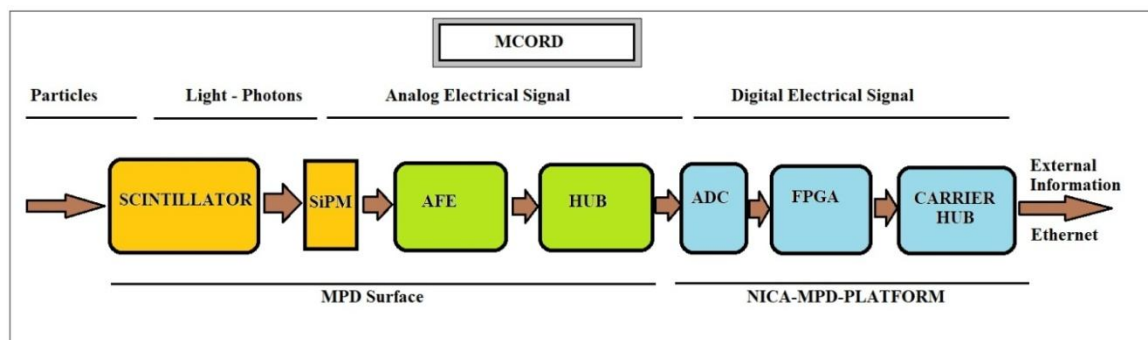


Figure 7 – MCORD idea scheme.

Analog front-end electronics (FEE) will pass signals from the SiPMs by the HUB to a digital electronic system based on Field-Programmable Gate Arrays (FPGAs) and implemented in MicroTCA (MTCA) standard. MTCA crates are located in racks on the NICA-MPD-PLATFORM. The system will enable real-time signal analysis and will produce trigger signals to other MPD subsystems.

The main features of the MCORD detector should be precise timing information, high detection efficiency for coincidence events, 2D positional sensitivity and cost-effectiveness (low price per unit module). However, fulfilling all these requirements pose contradictory constraints on the detector design. Therefore, not only the optimization but also some trade-off on the detector's performance is necessary.

The basic functional element of the MCORD detector will be the MCORD Section (8 scintillators) with control electronics (Figure 8). This means that each section can work as an independent detector and can be used for any type of measurement. The basic functional element of the MCORD detector will be the section with control electronics. This means that each section can work as an independent detector and can be used for any type of measurement. One section consists of the following elements:

- 8 plastic scintillators each with a wavelength shifting (WLS) fiber;
- 8 aluminum housings for each of the scintillators;
- 1 aluminum platform for mounting the scintillators;
- 8 AFE electronic boards;
- 8 USB-C cables;
- 1 passive HUB - voltage converter;

- 2 SAS cables + 1 SMA cable + 1 LAN cable;
- 1 AFC - FMB card;
- 1 MTCA crate;
- 1 PoE switch.

Please note that the last two items can be used to handle multiple sections at the same time.

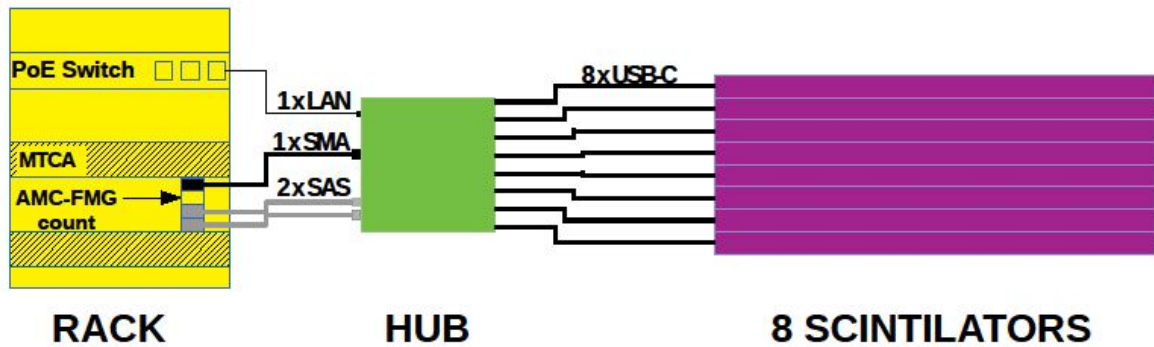


Figure 8 – Basic functional element of the MCORD:Section with electronic.

4.1.2 Mechanical Structure

When the conceptual work on the MCORD project has begun, the MPD detector design was nearly finalized. For this reason, the only possible location for this additional detector is the surface of the MPD housing. An additional limitation comes from the size of the MPD cradles supporting the construction and holes leading cables from the MPD interior. For these reasons, we proposed that the MCORD detector surrounds the MPD enclosure on its full perimeter limited by the support cradles (legs) structure (Figure 9). The MPD casing has the shape of a barrel with 28 walls. For this reason, the MCORD detector is divided into 28 parts that can be installed on the MPD surface as 28 modules. Each module can be installed independently on a separate frame (Figure 10).

Each of the modules consists of 3 sections (with 8 scintillators each). The two lateral sections are located at the same level, and the central one is slightly raised above the other two. The area covered by the sections coincides and thus there is no dead space between the sections (Figure 11). The weight of a single MCORD section (8 scintillators in aluminum housings + section frame) is about 50 kg, so the weight of a single module without a frame is about 150 kg. Technical drawings and images visualizing the elements of the MCORD detector (scintillators, sections, modules and mounting frames), along with all dimensions, will be reported in the MCORD TDR document. The upper part of the MPD barrel has a slightly different structure than the bottom. In the upper part there are regularly spaced holes to which we can attach structural frames for modules. There are no such holes in the bottom part, and additionally there are large clamps fixing the MPD supporting cradles (Figure 12).

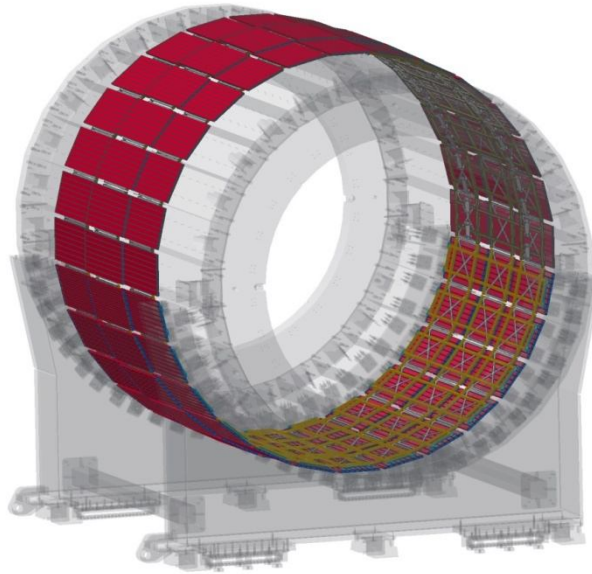


Figure 9 – The MCORD structure (in red color) on MPD surface.

A (1 :10)

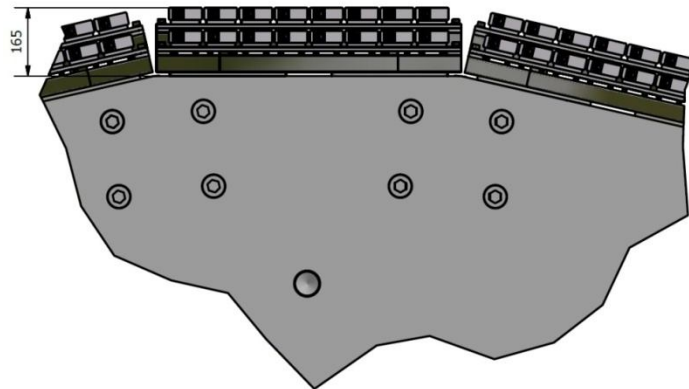


Figure 10 – Installation of MCORD modules on MPD surface.

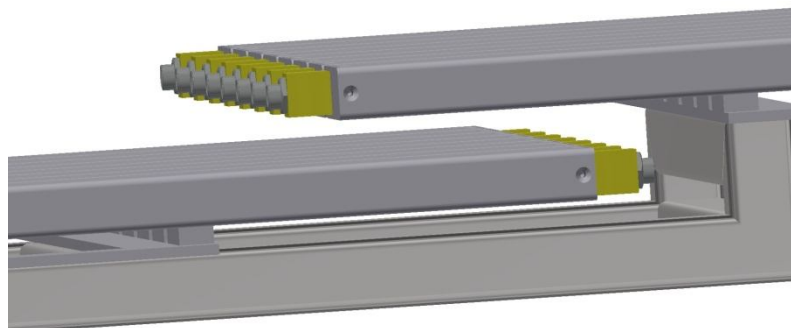


Figure 11 – The central section is above the two others.

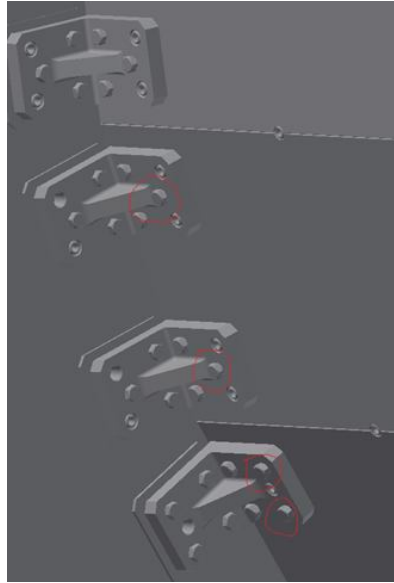


Figure 12 – Screws on the angle bars connecting the MPD drum to the legs.

The method of attachment of these angles is different (Figure 12). Some bolts protrude from the plane of the angle bracket, and some have threaded holes inside. We intend to use the drums with holes as a way of fixing the module frames in the lower part of the MPD. For these reasons, the mounting frames of the modules must be structurally different for the top and bottom. In the upper part of the MPD the frame can be attached to 2 x eight points located closer to the center of the frame (Figure 13), and in the lower part of the MPD barrel only to four points located at the ends of the frame. For this reason, the frame for the lower part will need to have a much stronger structure (Figure 14). After approving the method of fixing the modules to the MPD surface, the necessary calculations and simulations will be carried out, which will check the strength and deflection of the frame structure. Such simulations will be necessary because it should be remembered that the frames and modules are over 4 m long. The proposed material for the construction of the frame will be aluminum, but it may turn out that (due to problems with the strength of these structures), it will be necessary to use steel frames.

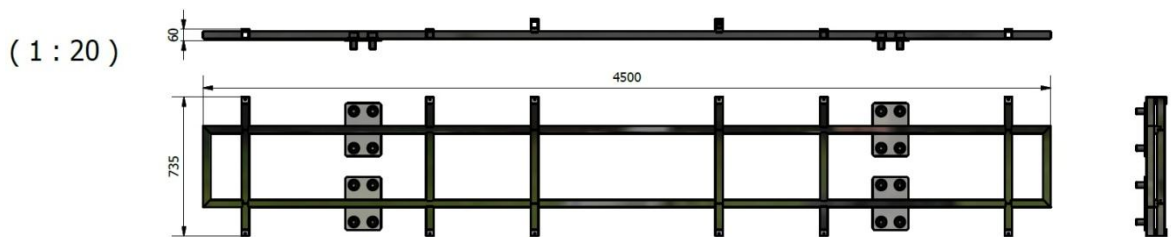


Figure 13 – MCORD module frame for the upper part of the MPD barrel.

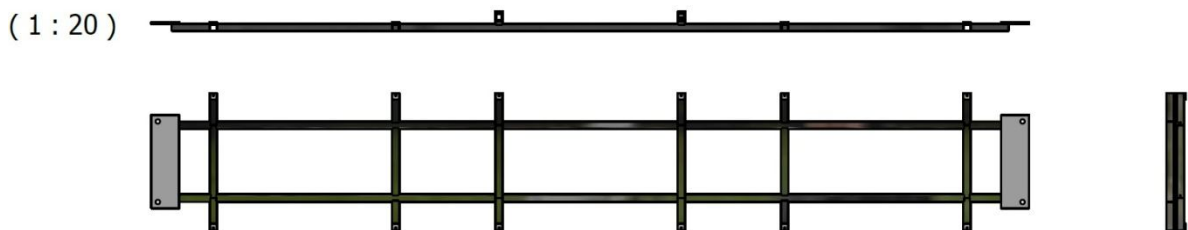


Figure 14 – MCORD module frame for the lower part of the MPD barrel.

4.1.3 Electrical Structure

The dataflow is presented in a Figure 15. There are two SiPMs dedicated for one scintillator. The analog output signals from two SiPMs go directly to the one Analog Front-End (AFE) module, which is located as close to the SiPMs as possible. Therefore, all AFE hardware modules are of high radiation hardness. AFE module is mainly responsible for monitoring and controlling SiPMs, electronic protection, temperature measurements, failure notifications etc. Additionally, it consists of a very simple amplifier and shaper. The role of the shaper is to form the pulse. Output pulses from this module have reduced bandwidth and thus increased duration. The bandwidth limitation reduces hardware requirements for a readout equipment and minimizes RF interferences.

Analog signals from the AFE are transmitted to the passive HUB (located near the detector). HUB can support up to eight AFE modules, which gives totally sixteen SiPM analog signals. There is no SiPM signal processing in the HUB module, which is mainly responsible for power delivering, controlling and transferring physical and diagnostic data from the AFE. The SiPM signals are transmitted from the HUB to the ADC (Analog to Digital Converter) and TDC (Time to Digital Converter) chips located on the FMC (FPGA Mezzanine Card) boards. Every FMC card receives 16 analog signals. In the next stage, already digitalized signals go from the FMC card to the AMC (Advanced Mezzanine Card) board. Each AMC board is connected with two FMC boards, which means that it can process up to 32 SiPM signals. Those digital systems (FMC and AMC modules) will be located on the special electronic platform (NICA-MPD-PLATFORM). Connection between the HUB and the platform needs long, high quality cables with a good resistance to noises and interferences. Therefore, for transmission were chosen standard SAS connectors and 24 or 32-channel cable. Each channel consists of a pair of wires where signals are transmitted in differential mode.

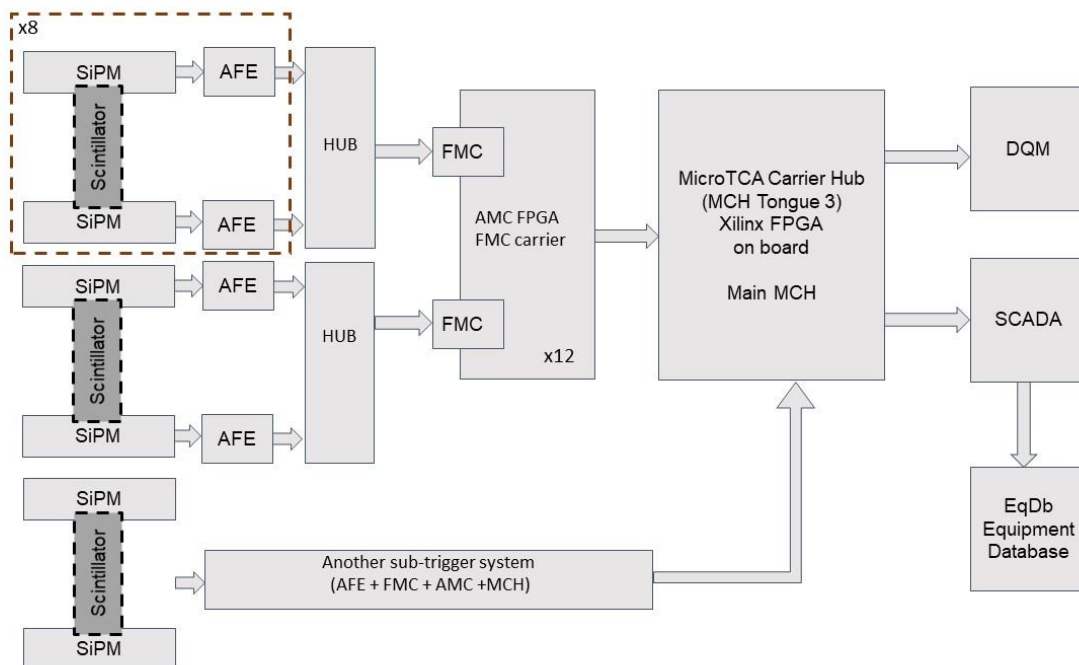


Figure 15 – System architecture based on MTCA standard.

AMC cards are installed in the system based on the Micro TCA.4 standard. This is a modular system for acquisition, control, management and data processing. The chassis

integrates embedded computer, management controller, PCIe Gen 3 and Ethernet hub. These features make it feasible for data acquisition and processing application in HEP (High Energy Physics) experiments.

The TCA standard allows installing up to 12 cards in the AMC standard. The industry standard of the AMC-FMC carriers are used for MCORD. An FMC (FPGA Mezzanine Card) is an ANSI (American National Standards Institute) standard that provides a standard mezzanine card form factor, connectors, and modular interface to an FPGA located on a baseboard.

In addition to the FMC and AMC-FMC modules, there is an MCH (MTCA Carrier Hub). The data, after processing in the AMC FPGA, are transferred using the MTCA backplane to the MCH module. The MCH has gigabit ports that enable connection of multiple crates into one system. The MCH contains a large Kintex FPGA which performs further processing. The whole system will consist of up to three MTCA crates. One of the three MCH FPGAs behaves as a hub that receives data from another MTCA crates using the 10Gbit serial link.

At the last stage, data from the MCH is transferred to two different blocks:

- DAQ (Data Acquisition)
All physics measurement data are sent to that database system. Main goal of the system is to perform various algorithms calculations on the delivered data to recognize the event parameters, its quality, rates etc.
- SCADA control system with EqDb Equipment Database
All diagnostic data is sent to that system in order to verify any failures in the system, detect unspecific behaviour and parameters or values beyond the limits. Additionally, the SCADA system can store all settings for SiPMs, which can be used during configuration of the whole electronic system.

4.1.4 Logical Structure

The logical structure shows the data and signals flow in the system and describes data service and handling. The diagram in Figure 16 presents the signal path. The signal is passed from the detector to the analog electronics, which processes the signal to prepare it for transferring to digital electronics. Analog electronics modules (AFE and HUB) can be managed, tested or calibrated directly by a properly trained person. This procedure is needed during initial tests, laboratory measurements as well as in the case of any failure or need to carry out diagnostic procedures. Diagnostics can be carried out using the USB, CAN or RS-485 bus.

Then the signal is transmitted to the digital part of the electronics, where the collected physical data is analyzed. This data is then saved in the DAQ database. In addition to data, the settings of the analog electronics are also transmitted. This information will be saved, via the SCADA system, in another database – the EqDb (Equipment Database). The reverse data transmission is also possible with this type of data. For example, in the case of automatic calibration of analog systems, the parameters of this calibration or reference values can be downloaded from the EqDb database and sent to the analog electronics module via the SCADA system. The SCADA system supervises the operation of all systems (analog and digital). Operators supervise and control the detector through the SCADA system. They use the specially written programs for that purposes.

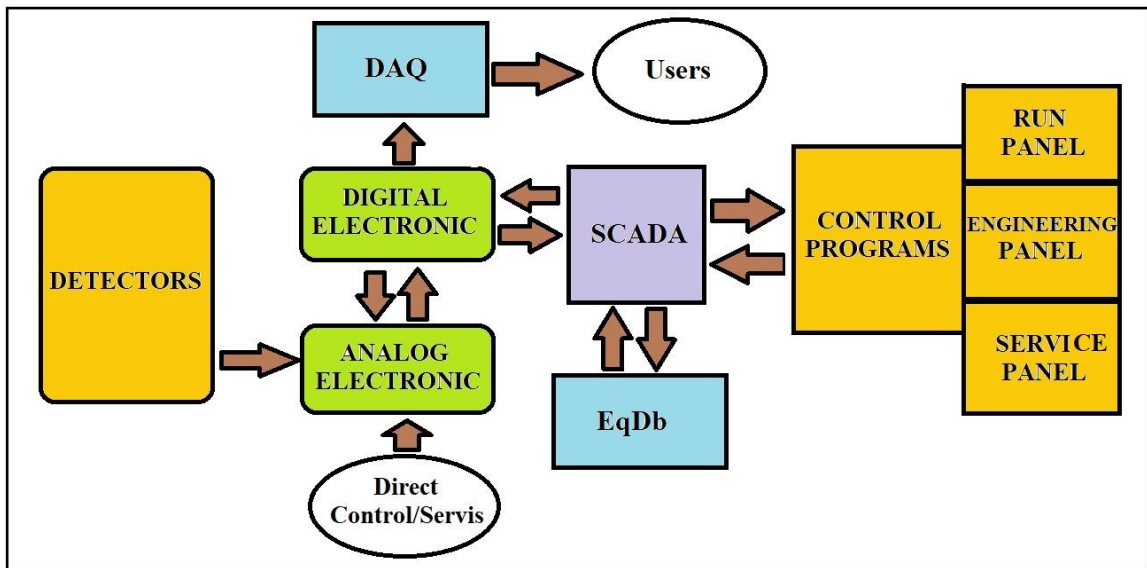


Figure 16 – Logic diagram of the MCORD detector.

The functionality of this software will be divided into three main parts. Access to individual parts of the software will depend on the user's privileges and will be controlled by an access password. The first module "Run Panel" will be the simplest part available to all users. It will perform the function of monitoring the detector status and display it on the control screen. Users will only be able to change the way this information is displayed without changing the detector's operating parameters. This panel can also include the emergency switch off function of the detector. The second module "Engineering Panel" will only be available to trained operators. In this panel it will be possible to start the detector and change the basic parameters of its work. Changes to these parameters, however, will be possible only to the extent that it does not endanger the correct and safe operation of the detector. The last module "Service Panel" is intended only for people who have full knowledge about all aspects of the detector. In this panel, it will be possible to carry out any service and diagnostic work. The user will be able to freely change all operating parameters.

The operators' work will be possible both from the control room located not far from the MPD detector, and from any point in the world through the WAN.

4.2 Scintillators and readout sensors

The MPD is a large size device of about 8 m in length and about 6 m in diameter. Therefore, surrounding the MPD with the MCORD requires to use the relatively cheap and efficient materials. The most common material for muon detection is plastic scintillator.

Concerning the detector cost, plastic scintillators are one of the best candidates for the MCORD's detection medium as they are one of the cheapest charged particles sensitive materials [14], [15]. They are relatively bright, provide fast scintillation pulses and can be produced in large sizes. To ensure 2D positional sensitivity we propose to use the long, narrow slabs of plastic scintillators with WLS fibers, and with double-sided light readout using SiPM photo-detectors. The time difference in light propagation through the plastic scintillator will be used to define the particle interaction point along the detector module, whereas the width and thickness of the slab will give limits on the muon track point in the plane perpendicular to the long detector axis.

The dimensions of a single scintillator bar are $1620 \times 72 \times 22 \text{ mm}^3$ (Figure 17). Each scintillator is equipped with a 1 mm or 2 mm diameter WLS fiber readout on both ends by a $3 \times 3 \text{ mm}^2$ SiPM. The plastic bars are covered with a metalized foil as a reflector and a black foil to ensure light tightness. All the wrapped bars are sealed in the aluminum rectangular profiles providing mechanical ruggedness and additional light leakage protection. The scintillators made of polystyrene were provided by NUVIA Company (Czech), whereas the SiPM were of the S13360-3075PE type, delivered by HAMAMATSU.

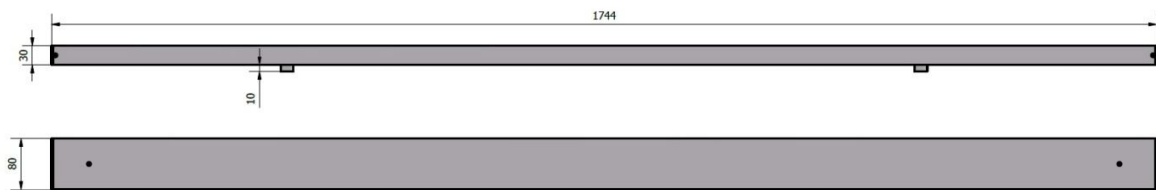


Figure 17 – Scintillator inside an aluminum cover.

Inside the aluminum cover, in addition to the scintillator at each end, the plates with the AFE electronics (SiPM's power supplies and amplifiers) will be placed. The both ends will be sealed with a special plug in which the USB port will be located (Figure 18). Both the plug and the USB port will be dust and light tight, so the scintillator material will not be exposed to the dust and moisture and will keep its original parameters for a very long time.

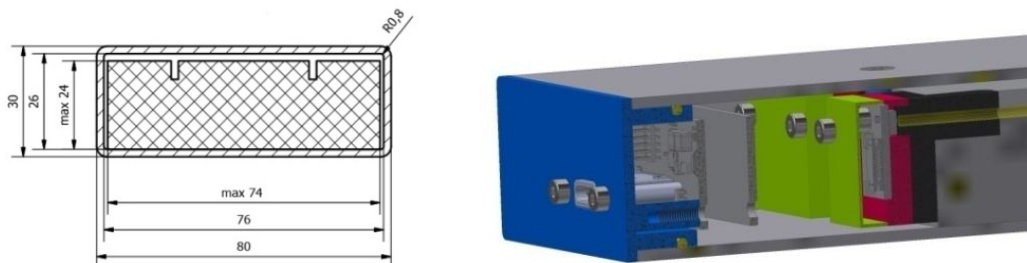


Figure 18 – Cross-sections of single detector with aluminum cover.

Legend for right picture: blue – the end cap with USB port, gray – AFE electronic plates, green and red – cover for plate with SiPM, black – connector for fiber on the end of scintillator.

The bars are subsequently assembled into sections comprising of the 8 pcs. each (Figure 19). Every section could be used separately, e.g. during laboratory tests with other detection subsystems or grouped into modules comprising three sections (Figure 20). We propose the latter configuration to use for surrounding the MPD, where the MCORD modules will be arranged in a barrel shape around the central part of the MPD detector as visualized in Figure 21.



Figure 19 – Scintillator assembled into a section comprising 8 detectors.

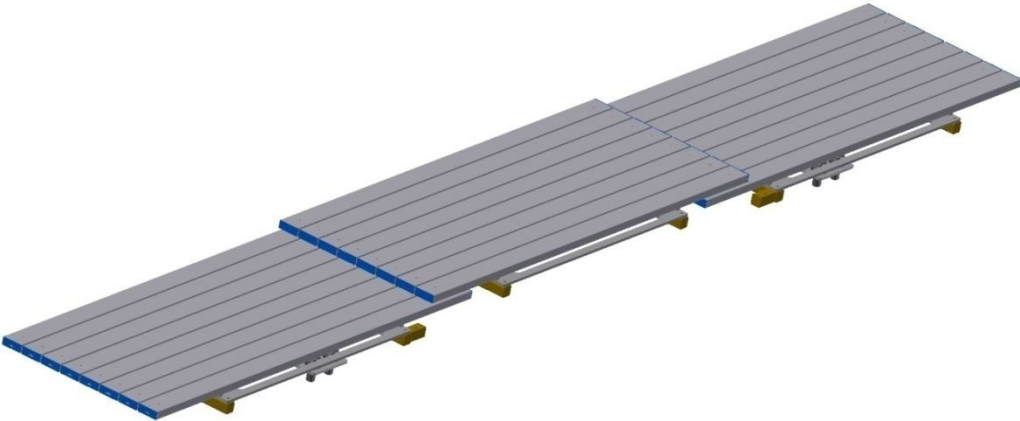


Figure 20 – MCORD muon detection module.

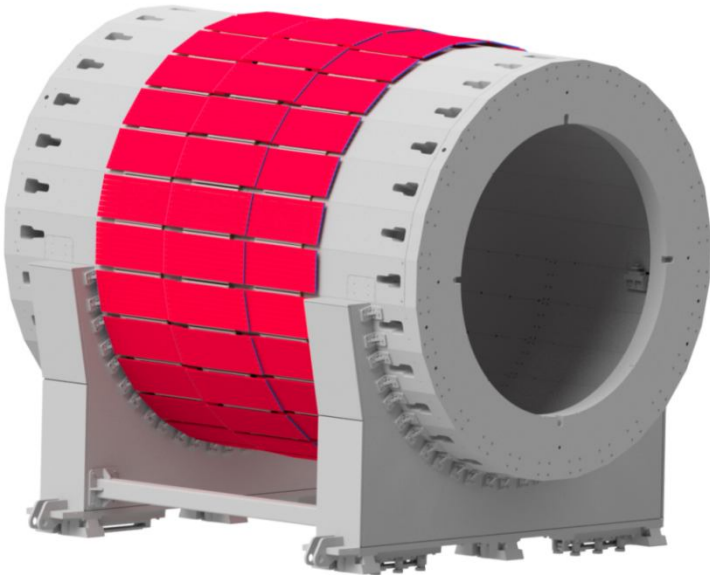


Figure 21 – MCORD installed around the MPD.

In the presented design of the MCORD it is foreseen to install 28 modules of 24 scintillator bars each, however the system is functional also if built from smaller number of the modules. In such reduced configuration it could be already used for calibration of the MPD subsystems already after assembling in the service position, before first in-beam tests. The feasibility study of MCORD configurations for the test measurements and the first off-beam calibration of the MPD subsystems will be presented in subsection 5.2.

4.3 Readout Electronics

An analog readout electronic is built from two modules – AFE and HUB. The AFE (Analog Front End) is connected directly to the SiPMs and is placed very closely to them. In the final solution, part of the AFE with amplifier and power supply will be moved away from a SiPM due to decreasing the AFE influence on the SiPM's work temperature. Additionally, temperature sensors will be installed very closely to the SiPM sensors (at distance up to few millimeters). The basic functionality of the AFE is depicted on the schematic in Figure 22. One AFE board cooperates with two SiPMs dedicated for one scintillator.

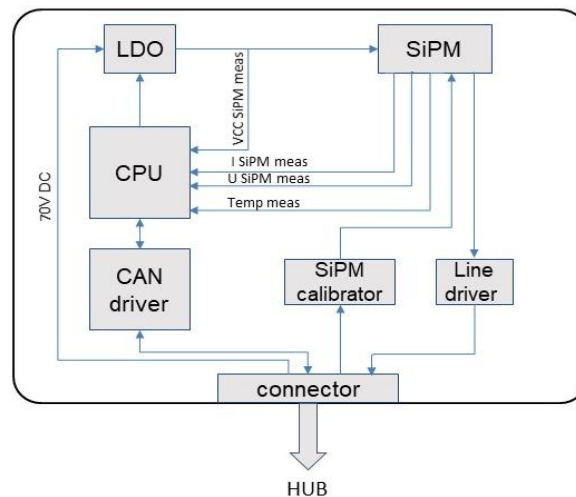


Figure 22 – Basic functionality of the AFE module.

The heart of the AFE module is a STM32 microprocessor. The software is written in an ANSI C language. The GCC tool chain is used for development. The microprocessor is responsible for managing and controlling of all on-board and SiPMs hardware parts:

- Two temperature sensors of the SiPMs
- Two LDOs (Low-Drop Out regulator) dedicated for the SiPMs voltage controllers
- Two SiPMs calibration blocks
- Two SiPMs signal transmitters
- CAN network driver (Controller Area Network [16])
- External memory interface for remote firmware update

An AFE is connected with the HUB by the connector where are available the following signals:

- CAN interface (both directions)
- Calibration signals (to AFE)
- SiPMs analog signals (to HUB)
- Power (to AFE)

The AFE communicates with a HUB by the CAN interface, which provides access to all AFE settings and data. Each AFE node has a unique CAN identification address (Message ID). The communication protocol is open and available for all users.

The power supply (up to 70V) for the SiPMs comes from the HUB and is controlled by the AFE in a control loop. Microprocessor monitors the following parameters and based on those values it controls and, when necessary, adjusts the SiPMs operating points by changing the settings of internal DACs (Digital to Analog Converter) outputs:

- Supply voltage of each SiPM,
- Current of each SiPM,
- Voltage of each SiPM,
- Temperature of each SiPM.

Besides controlling the SiPM, the microcontrollers perform other tasks:

- Probing current-voltage characteristics to identify damaged SiPM and switch them off
- Controlling the SiPMs calibration procedure to set correct operating points,
- Transferring analog signals from SiPMs to the HUB,
- Controlling procedure of update firmware by CAN interface.

The second part of the analog readout electronic is a passive HUB module. To one HUB up to 8 AFE modules can be connected. The main functionality of the HUB is depicted in Figure 23.

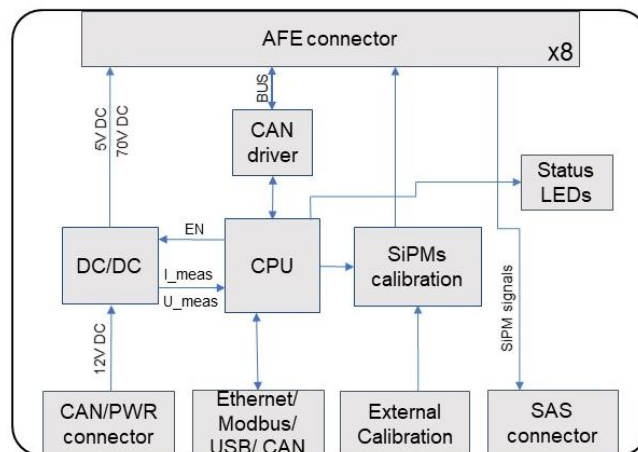


Figure 23 – Basic functionality of the HUB module.

STM32 microprocessor placed in the HUB is responsible for the following tasks:

- Controlling power delivery to the AFE boards (5V, 70V),
- Controlling the CAN interface for the AFE boards,
- Generating the calibration signals to the AFE boards or distributing the external one,
- Distributing analog signals from AFE to MCA boards,
- Controlling the Ethernet/ModBus/CAN/USB interfaces,
- Managing status LEDs on the AFE and HUB for quick fault identification,
- Storing diagnostic data in the external memories,
- Controlling procedure of the firmware update.

The HUB is supplied by a PoE standard device, which can deliver 12V. The HUB contains the DC/DC converters which transform 12V to 5V and 70V. Those voltages are then delivered to the AFE boards.

The HUB transfers analogue signals from the AFE to the next stage MCA (Micro Channel Architecture) card without and additional process. The HUB software is responsible for delivering and receiving parameters, settings and data to/from the AFE boards. Additionally, it informs about any errors occurring on the AFE boards.

Microprocessor placed in the HUB runs the MicroPython compiler. This is a Python programming language optimised to run on the microcontrollers and in the constrained environments. The whole software and all functionality of the HUB will be developed in that language. After connecting the HUB to the PC, it emulates the USB disk. This approach allows to develop control or diagnostic routines by non-embedded software engineers (i.e. physicist). MicroPython gives a simple access to CAN interface and functions to communicate with the AFE modules.

4.4 Digital Electronics (FPGA)

Analog signals from the SiPMs are passed from HUBs to the next stage – the FMC boards located on the AMC-FMC cards (Figure 24)(Advanced Mezzanine Card - FPGA Mezzanine Card). On the FMC card the signals are processed in two ways: by the ADC (Analog to Digital Converter) chips and the TDC (Time to Digital Converter) chips. Both paths work simultaneously and can support up to 16 channels. Due to many FMC boards working in parallel, timing synchronization is available. The board can work with internal or external clocks.

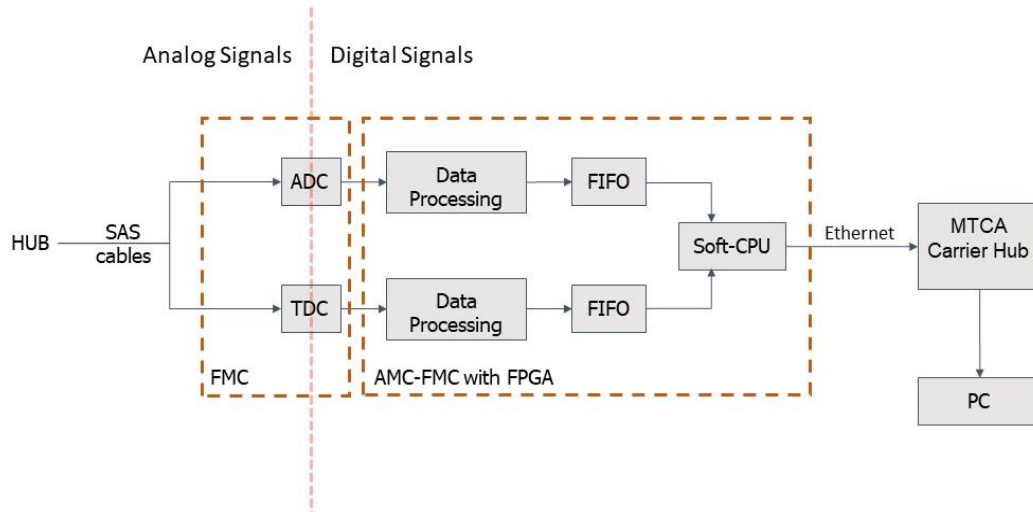


Figure 24 – Dataflow on FMC and AMC boards.

The ADC digitizes the signals and sends them to an FPGA chip. The ADC path basically has to stretch the incoming signal. Because the signals are very narrow, the conversion process would need chips with very high sampling rate. To reduce that requirement, the signal is stretched before quantizing.

On the other hand, the TDC processing is a very precise method to detect edges of the signals. The TDCs calculate times of incoming samples with very high resolution.

At the next stage the digitized signals coming from the ADCs and TDCs are transferred to FPGA (placed on the AMC-FMC boards) where they are initially processed.

Both digitalization methods play a big role in a data processing, because each method stores the different information. The ADC digitalization allows to calculate the charge and energy of the signal, its quality, correlation between various pulses and other parameters. The TDC digitalization allows to precisely calculate the position trajectory of the muons, time of arrival, time difference between scintillators both ends.

Two FMC modules can be connected to the AMC-FMC boards. It means that each AMC-FMC board can support up to 32 analog signals from the SIPMs. Boards can be synchronized to each other with nanoseconds precision. The data after processing in the AMC FPGA are transferred using the MTCA backplane to the MCH (MTCA Carrier Hub) module(Figure 25). MCH contains the large Kintex FPGA which performs further processing. Data from MCH can be processed finally to the PC over the Ethernet connection.

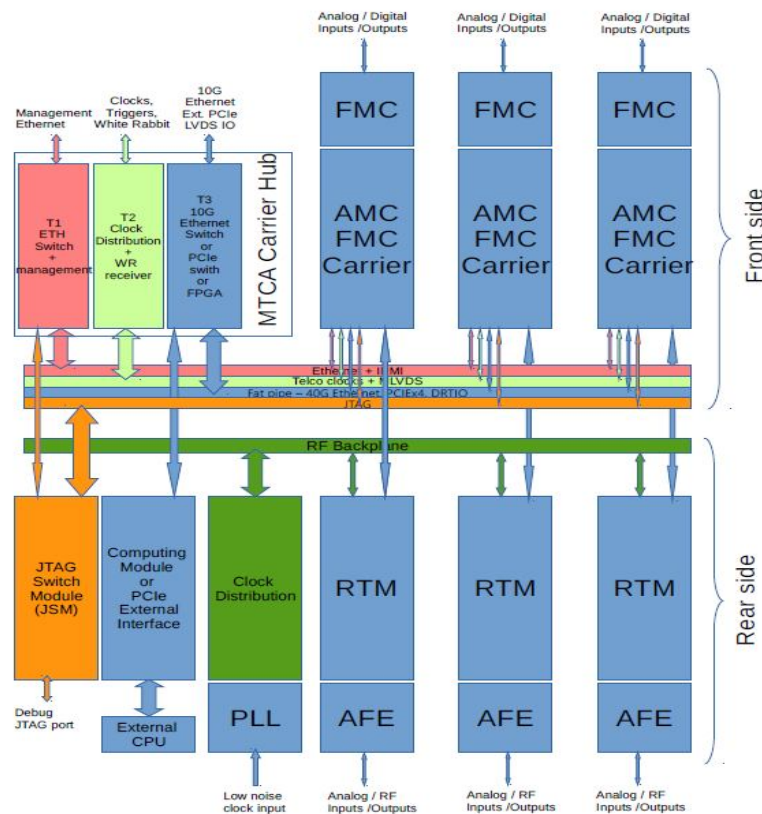


Figure 25 – Architecture of MTCA crate, ver. 4.

There are other optional modules which can be mounted in the crate. They can be used for future upgrades of the system. The T2 Clock Distribution module enables the use of the White Rabbit [17] standard to synchronize multiple AMCs and MTCAs with sub-ns accuracy. The JTAG Switch Module allows remote debugging of the FPGA devices. This is useful during the software development, it enables remote access to the system installed in the tunnel or experimental area under radiation conditions. The RTM (Rear Transition Module) module will not be used in this experiment.

4.5 FPGA Based Muon Trigger

The muon trigger, implemented in the FPGA, utilizes signals produced by the photon-detectors connected at both ends of the scintillator strips. The signals are shaped by an amplifier and converted to the digital form using the ADC and TDC converters.

The digitized signals will be processed in the FPGA to calculate the time and amplitude of signals at both ends. The position of the hit along the scintillator is calculated from the time difference between those signals.

The track and direction of the muon will be calculated in the FPGA based on the coincident hits from different detector layers. The fast and low latency process of a muon's trajectory identification will be based on the muon trajectory processor original concept for the Overlap Muon Track Finder in the CMS (Compact Muon Solenoid) muon trigger system [18], [19].

It is planned that our system could generate three types (levels) of the trigger signals. They will differ in latency and accuracy. Level one trigger signal will convey information that the event occurred without specifying its exact parameters, with a latency of several hundred nanoseconds. The third level trigger signal will provide full information about the signal obtained after its full analysis, with a latency of 5-15 microseconds. The given values are based on the potential possibilities of electronics and are not based on the designated properties of scintillators.

4.6 Requirements

All external requirements and connections of the MCORD with the MPD technology, databases and software will be described here.

4.6.1 MCORD integration with MPD

The main components of the MCORD detector are to be placed on the surface of the MPD. For this reason, no cables are routed inside the MPD. The MCORD detector requires that most of the MPD barrel surfaces be reserved for installation. Specifically, the entire area bounded by the legs supporting the MPD barrel is required minimum (see drawings and descriptions in sections 4.1.2, 4.3). The MCORD module will be installed on this surface through the mounting frames. In addition, more space may be needed at the top of the MPD barrel for attaching the HUB boxes and the cable channel going from the MPD detector to the platform (Figure 26). When the reservation of this additional space will not be possible, it is considered that the HUB modules and cable channel should be placed on the surface of the MCORD modules in its final part. However, this solution is not recommended because it will make access to the MCORD section very hard and will make any repairs or replacements very difficult. Replacing a single AFE module or scintillator may require disassembly of the entire channel with cabling and the HUBs (Figure 27).

On the MPD surface, the MCORD detector must be able to connect to independent ground lines for the aluminum cover and aluminum mounting frames.

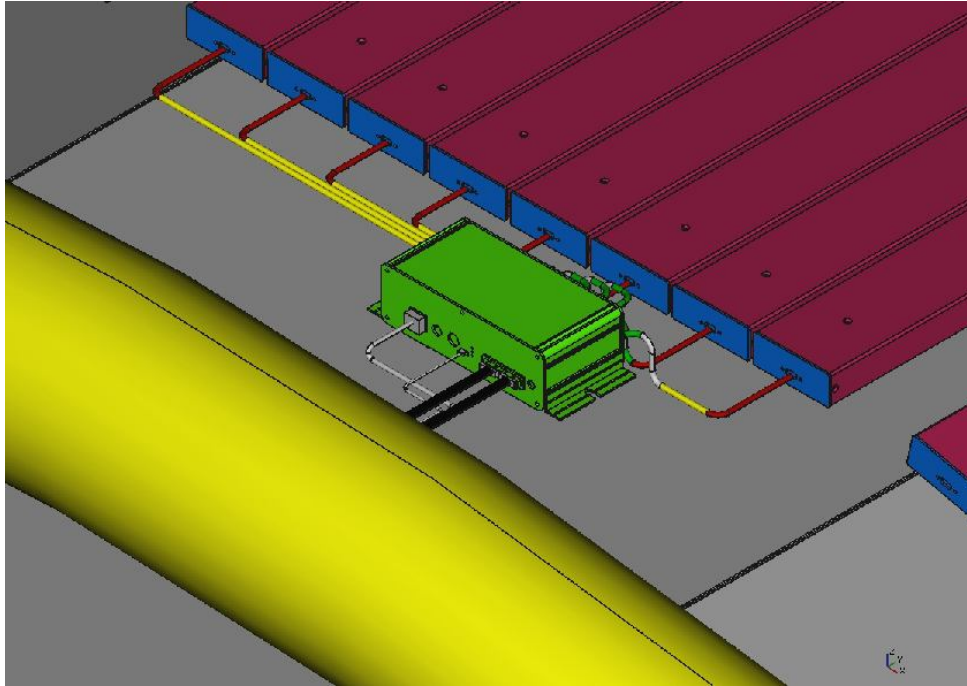


Figure 26 – MCORD module, HUB and cables system on the MPD surface.

Cable channels and HUBs are located next to the MCORD modules.

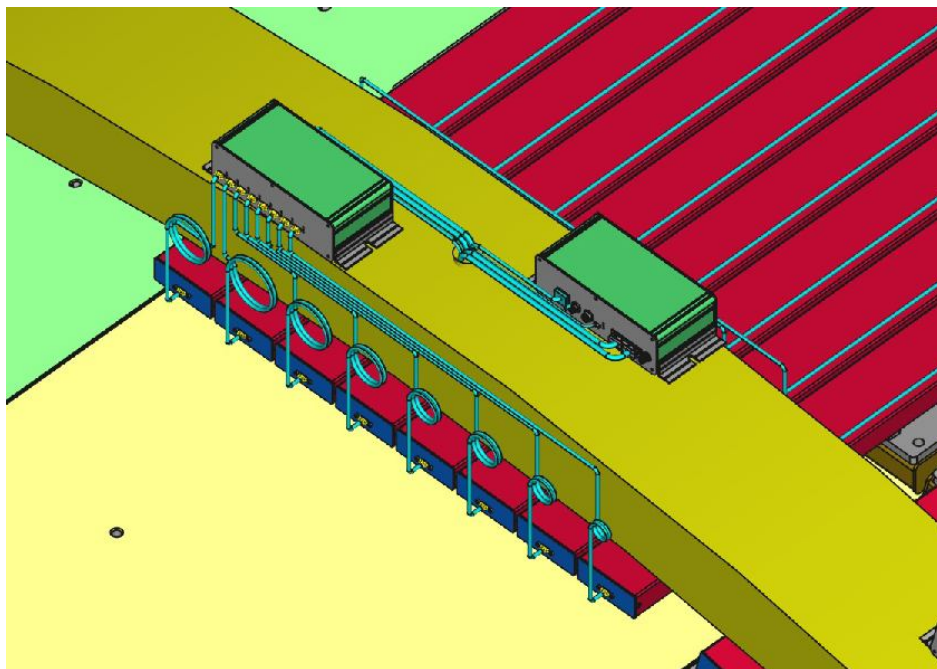


Figure 27 – MCORD module, HUB and cables system on the MPD surface ver.2.

Cable channels and HUBs are located on MCORD modules.

4.6.2 Cable Routes

The cables collected in the MCORD detector cable channel must be routed to the NICA_MPD PLATFORM. The path through which these cables can be routed must be included and sufficient space must be reserved for this extra cable bundle. Due to the fact that the MCORD detector is located on the surface of the MPD barrel, the cables from this detector can be routed to the NICA_MPD-PLATFORM in the same way as other cables

from other detectors us the channel located on the edge of the barrel circumference, or they can be routed through a separate special dedicated channel for the MCORD detector (Figure 28). It should be remembered that the electronics boxes for the TOF detector will also be located on the surface of the MPD, and for this reason routing an additional channel to the NICA-MPD-PLATFORM for the MCORD detector cables can be a simple solution.

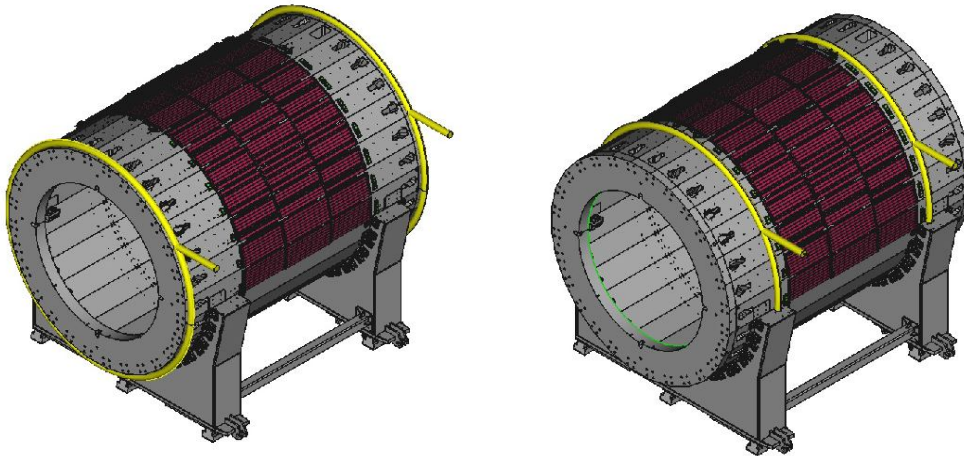


Figure 28 – Cable routes from the MCORD to the NICA-MPD-PLATFORM.

Left: along with other cables. On the right: a separate dedicated channel.

The full analysis of the number of cables from the MCORD system going from the MPD to the NICA-MPD-PLATFORM will be describe in the TDR document. From a single MCORD section we have eight USB-C cables between scintillators and MCORD HUBs and from the HUB will have the two SAS, one LAN and one SMA cables. These four cables go from each section to the NICA-MPD-PLATFORM on which the racks with MCORD digital electronic components are located.

4.6.3 User Space in NICA-MPD-PLATFORM

The NICA-MPD-PLATFORM will be fitted with rack cabinets for detector electronics. Each rack has 35U free space (standard units of space in the racks). The rest is used by standard equipment like power supplies, cooling, fire protection equipment (NICA_MPD_PLATFORM systems).

The signals for the MCORD detector will be transmitted through the cable system described in the previous chapter. These cables will be connected to the digital modules of the MCORD system, which includes the MTCA crate and the PoE switches. A full MCORD detector will require 4 MTCA crate and 4 PoE switches with 24 ports each. We need two, not fully loaded, racks for those equipment.

4.6.4 Power Requirements

As it was described in the earlier chapters, all the necessary power supply for the MCORD detector components located on the surface of the MPD barrel is transferred there via LAN cables going from the PoE switch. So, these devices do not need any additional power cord. The power required by the MCORD detector therefore only applies to components on the NICA-MPD-PLATFORM. A list and description of these components can be found in the previous chapter. From this description we know that the MCORD detector needs 4 MTCA crate and 4 PoE switches witch maximum rated power of about

500W each. A detailed description of the required maximum power will be described in the TDR document.

4.6.5 MCORD integration with SCADA WinCC

The management and supervision over the functionality of all the MPD components as well as the MCORD detector will be implemented by the SCADA system. The SCADA system will supervise all detector parameters except for recording the physical data from the measurements. Many other systems can send different types of alarm signals. The SCADA system will relay the information about these events to the operators of other systems. The information necessary to properly start and calibration of the detector will be stored in the EqDb database and use when it will be necessary by the help of SCADA system. The exact principles of cooperation with the SCADA system will be determined at a later date, when the documentation and assumptions for the operation of the SCADA system for the MPD will be developed.

4.6.6 DAQ Data Acquisition

Preliminary description of signal parameters which will be stored and MCORD communication with MPD Data Acquisition System (MDAS) will be described below.

The raw data available from the MCORD readout electronics include a few basic parameters related to detected signals and the FEE settings at the time of event detection. The raw data will be used to provide required information about the detected event. The FEE settings are stored for detector performance monitoring and eventually, for offline data recalibration. The example of information passed to the MDAS are: detectors ID, voltage set on each SiPMs, temperature, amplitudes of signals detected each SiPMs, timestamps of signals and based on the amplitudes and timestamps recorded, the subsequent information are evaluated and passed to the MDAS like: amplitudes, timestamps of the events detected in a scintillator bar and points of the interactions in a scintillator bar.

In case it is required to use the MCORD modules in high count rate measurements, when multiple hits in one scintillator bar could be registered, the information about the most probable number of particles detected during event recording will be evaluated [20].

The structure of the data records sent to the MDAS will be defined after the guidelines for the data transfer and storage are announced.

4.6.7 EqDb Equipment Database

The EqDb database [21] with the SCADA control system will be responsible for managing and controlling the detector configuration. Additionally this system will receive, store and process the diagnostic and calibration data. The information to be saved in EqDb database will be provided by the analogue part of the MCORD system, i.e. from the AFE and HUB modules.

5 Evaluation

During the development of the large-scale systems like MCORD, simulations of the muon interactions with scintillators, building walls, and the detector elements are required to estimate the system performance. For that purpose, simulations were performed to obtain information about:

- energy and angular distributions of particles considered as “cosmic rays” reaching the MPD;
- energy and angular distributions of cosmic muons able to pass through the MPD (taking into account interactions with the MPD detector yoke and solenoid);
- muon tracks that could be used for MPD subsystems calibration;
- energy and angular distributions of muons and other charged particles generated during collisions that could escape from inside of the MPD.

Energy distribution and composition of the cosmic radiation were calculated using simulation code CORSIKA [22]. The interactions of muons with the MPD detector were calculated using GEANT3 and 4 code [23]. The influence of the walls on the muon flux reaching the MPD has been found negligible.

In parallel, as production of the detectors is carried on, laboratory characterization and optimization of performance is performed. The results presenting the current status of the development are reported in the following subsections.

5.1 Cosmic Shower Simulations

Investigation of composition of ultra-high energy cosmic rays and behavior of particle interactions at energies beyond those currently accessible at particle colliders can only be done by interpreting air shower experiments. Monte Carlo air shower simulation programs are essential tools for the analysis of data from cosmic ray experiments and for planning the layout of new detectors. They are used to estimate the energy and mass of the primary particle. Unfortunately, the model uncertainties translate directly into systematic errors in the energy and mass determination. Aiming at energies $> 10^{19}$ eV, the models have to be extrapolated far beyond the energies available at accelerators. On the other hand, hybrid measurement of ground particle densities and calorimetric shower energy, as will be provided by MCORD, will strongly constrain shower models. While the main uncertainty of contemporary models comes from our poor knowledge of the (soft) hadronic interactions at high energies, also electromagnetic interactions, low-energy hadronic interactions and the particle transport influence details of the shower development.

In practice, the main astrophysical magnitude observed will be multi muon events. Specifically, the multiplicity of such phenomena in relation to the number of muons in a single event. These types of phenomena were observed in the past in similar experiments and in particular in the ALICE, DELPHI, and ALEPH projects [25], [26], [27]. The main difference of the NICA-MPD experiment compared to those mentioned is the fact that they were located deep underground which naturally limited the energy and direction of the arriving particles. In the case of MPD, it will be possible to observe cosmic showers from directions even close to the horizon [28]. This type of observation of the cosmic shower from the horizontal direction with the participation of a large detector equipped with a TPC detector has never been performed in the past. Thanks to this it will be possible to observe much more phenomena of multi muons events than in the experiments in the past. It is the very low statistics of such extreme phenomena that are the main reason for their good

explanation. An additional very promising benefit may be an attempt to identify the location of cosmic-ray sources of extremely high energy particles and a potential explanation for the GZK Cutoff problem [29], [30].

During development of the large-scale systems like MCORD, detailed simulations of the production of hard (muons, hadrons) and soft (electrons, photons) components in the Extensive Air Showers initiated by primary protons and heavier nuclei are essential. We plan to estimate fluxes and energy distributions of muons, secondary protons, electrons and photons as a function of emission zenith angle. In order to set the optimal values of parameters used for simulations we plan to compare our simulations with the existing data on particle production in Extensive Air Showers obtained recently by the ALICE and other experiments at CERN in their dedicated cosmic ray runs.

Figure 29 presents simulated angular distributions of some particles from cosmic showers in a region near Dubna city. The presented distribution applies to particles with full energy distribution above indicated thresholds of 0.1 GeV, 1 GeV, 10 GeV and 100 GeV. It is worth noting that the distributions become independent of the zenith angle of primary particle for high energy secondary particles. Figure 29 shows also dominant role of muons in the particle flux. The numbers of protons and neutrons become significant only when we consider secondary particles with much lower energy than 1 GeV.

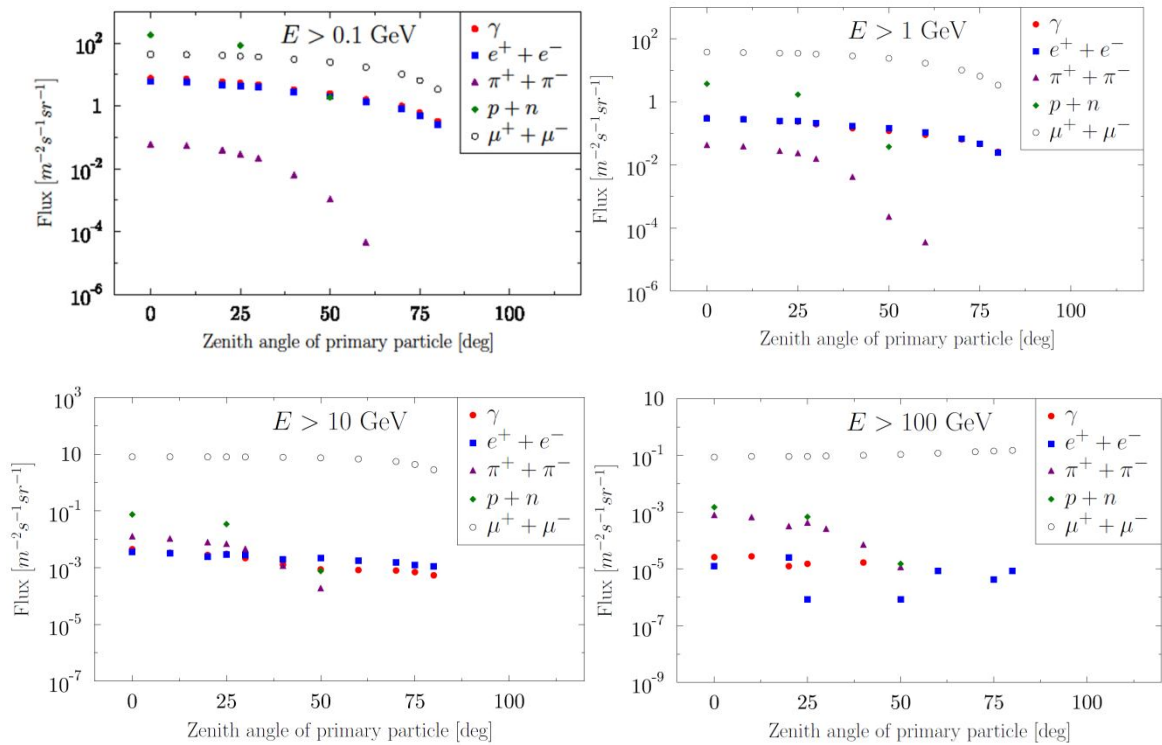


Figure 29 – Angular distributions of Extensive Air Shower components.

Location near and see level at Dubna city, with energies above fourth thresholds.

It is known that primary particles flux is dominated with protons and their energy distribution at energy range above 1 GeV decreases as $\sim E^{-2.7}$ [31]. On the other hand, the average number of muons per one primary particle as a function of its energy increases as presented in Figure 30. As one may note, cascades from primary protons with energies less than 100 GeV contain on average less than 1 muon at the detection level. Having the data presented above, one may calculate angular-integrated muon flux at ground level as a function of zenith angle of incoming primary particles, as presented in Figure 31. A brief

estimate of number of muons with $E > 1$ GeV reaching the ground is about $120/\text{m}^2/\text{s}$. The presented results were obtained using the Corsika 7.74 code (model QGSJETII-04 + UrQMD).

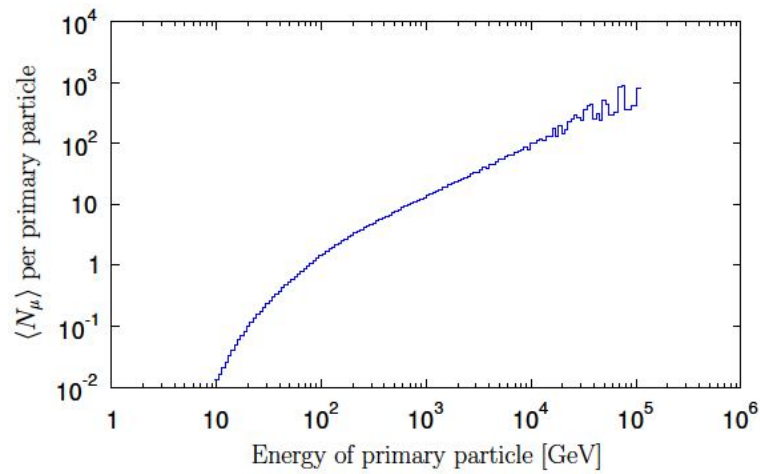


Figure 30 – Average number of muons per one primary particle.

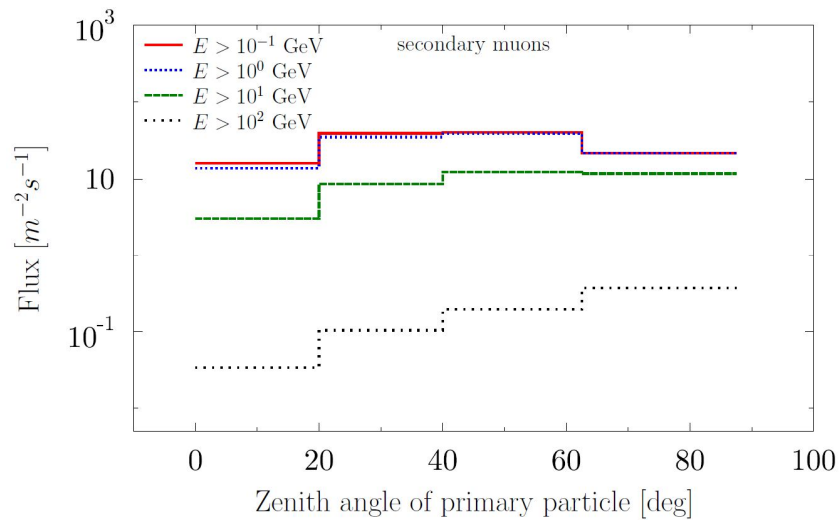


Figure 31 – Angular distribution of muons from EAS.

Location near and see level at Dubna city, with energies above fourth thresholds.

Since the MPD comprises a large magnet composed of a yoke and a solenoid, there will be some threshold energy for muons able to pass through the MPD and hence, to interact with modules placed on both sides of the MPD detector. Considering MPD subsystems with stopping power significant for muons, ECal should also be taken into account if muon energy threshold is calculated. To study the propagation of cosmic rays in the MPD detector a special version of *MPD root* was created. This version was based on the official *MPDRoot* dated June 2020 with a virtual “floor detector” added. The “floor detector” was placed 350 cm below the beam axis (few centimeters below MCORD). This detector was implemented just as a counter for particles that were able to reach it. The propagation of cosmic muons was simulated by directing downward a beam of muons from a point placed 750 cm above the center of the MPD (see Figure 32). The simulation was performed without presence of magnetic field. The transmission coefficient (i.e.

“transparency”) of the MPD was calculated as a fraction of muons that reach the “floor detector”.

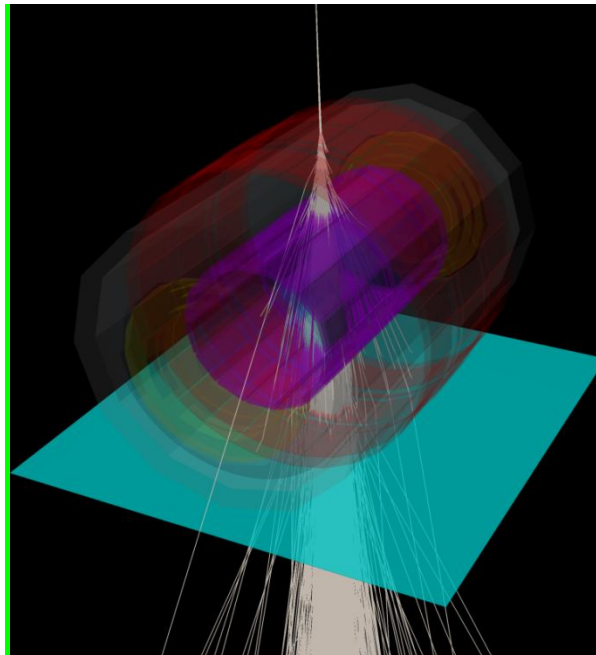


Figure 32 – To study the propagation of cosmic rays in the MPD detector.

The structure of the modified MPD detector. The entry point “floor detector” is represented by cyan color. The trajectories are represented by white lines. Red color corresponds to MCORD, the ToF detector is marked with purple.

Figure 33 shows energy dependence of muon transmission coefficient for MPD with and without ECal assembled. Assuming requirement for muon transmission above 95%, the muon cut-off thresholds are 1.6 GeV and 2.0 GeV, respectively. These results serve as an input for calculating the count rate for muons passing through the MPD that could be used for calibration of the MPD detector subsystems (e.g. ToF or TPC). The resulting energy threshold value of 1.6 GeV (in the absence of an ECal detector) from these simulations is used in the calculations presented in paragraph 5.2 (MPD subsystems calibration).

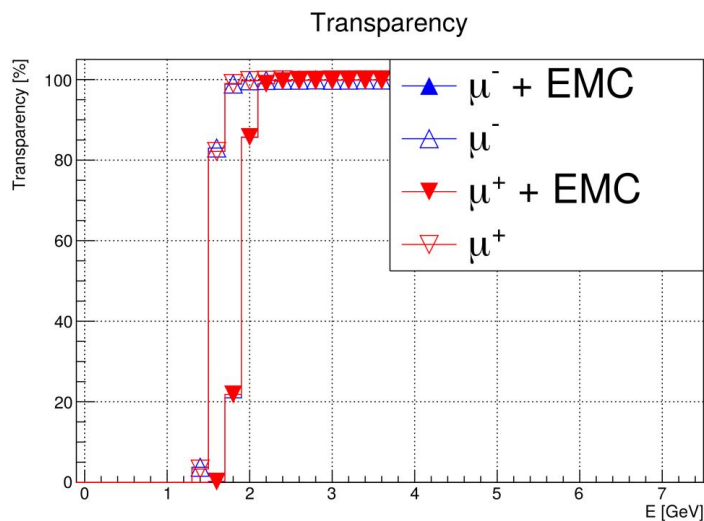


Figure 33 – Energy dependence of muon transmission coefficient.

Dependence through the MPD detector with the ECal (EMC) detector (solid triangles) and without (empty triangles) the ECal (EMC) assembled.

Simulations with full MPD detector were also used to estimate the “effective rescattering angle”. This angle is defined as an angle between initial direction of a muon and the line that connects two points: interaction of a muon with the upper MCORD layer and with the entry point “floor detector”. Non-scattered muons would have $\theta_{eff} = 0$. The results of these simulations are presented in Figure 34 and Table 5. As expected, the higher muon energy, the less deviation of the track from its initial direction.

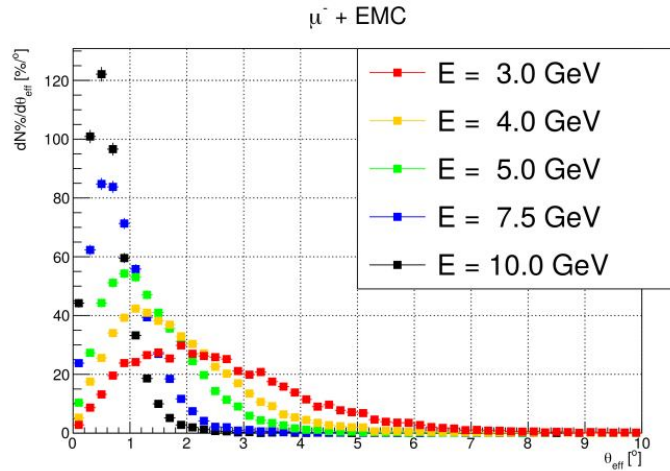


Figure 34 – Normalized distribution of the effective angle of muons rescattering. Inside the MPD detector with ECal assembled.

Table 4 – Effective rescattering angle for muons with different Energy thresholds passing the MPD.

| μ Energy[GeV] | $\langle \theta_{eff} \rangle$ | |
|-------------------|--------------------------------|--------------|
| | with ECal | without ECal |
| 3 | 2.68 | 2.24 |
| 4 | 1.85 | 1.65 |
| 5 | 1.41 | 1.31 |
| 7.5 | 0.91 | 0.87 |
| 10 | 0.65 | 0.63 |

5.2 MPD subsystems calibration

Simulations of muon events that could be used for MPD subsystems calibration were done using Cfluxim – a cosmic ray simulation tool. Cfluxim is a tool designed to generate tracks of cosmic secondary muons passing through a detector in a unit of time. The tool was developed to estimate time needed to calibrate detector modules using cosmic muon tracks. However, it may be used also in other applications. The following assumptions were applied for the current version of the tool:

- particle tracks are straight lines,
- interactions of cosmic muons with detector material is neglected,

- decays of muons are neglected,
- momentum distribution of the particles does not depend on zenith angle.

The tool is not capable of simulating interactions with detector material, decays, or track bending inside magnetic field. For more sophisticated simulation, cosmic flux generated by Cfluxim should be introduced into GEANT4 package simulation.

The tool generates particles that pass through a hypothetical cube of defined size. Each particle is defined by its momentum vector and initial position on one wall of this 'generation cube'. Particle initial position on the generation cube wall is drawn randomly from uniform distribution. To draw a momentum vector, the particle generator uses as an input data measured cosmic muon flux as a function of zenith angle [32] (Fig. 35) and measured momentum distribution of cosmic muons [33] (Fig. 36).

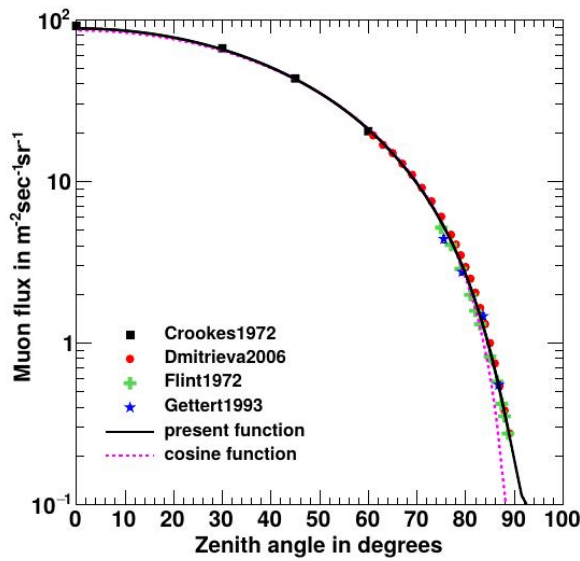


Figure 35 – Cosmic muon flux as a function of incident muon zenith angle.

Location at the sea level. The 'cosine function' is given by the following equation: $\Phi(\theta) = 10 \cos^2(\theta)$.

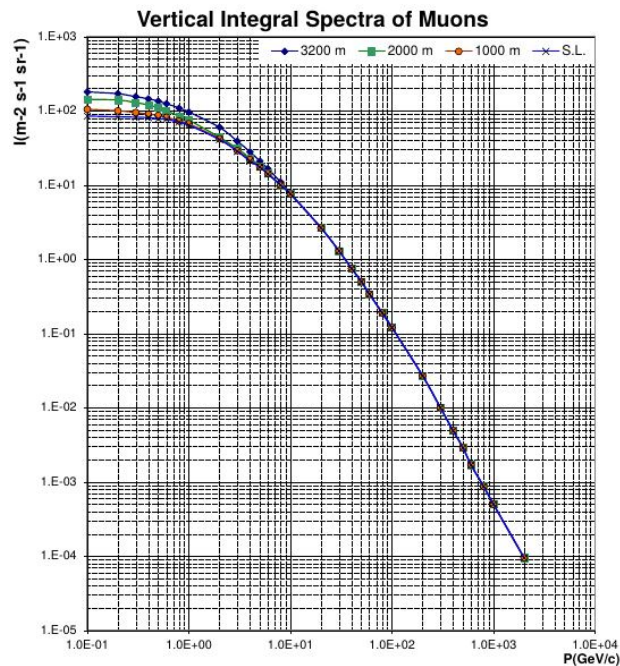


Figure 36 – Momentum integral spectrum of cosmic muons.

Each simulation was performed for 1 h acquisition time. The minimum momentum was set to $p_{min} = 0.1$ GeV/c. Detector was defined as a set of simple shapes: rectangles, disks and cylinders. The shapes must be defined inside the generation cube of 8 m edge. The analysis procedure was checking event-by-event which modules were crossed by particle trajectory. For each particle, the information if (and where) the detectors were hit was saved in an output file. Simplified geometry of MCORD, ToF and TPC was considered with the following assumptions:

- a. MCORD (see Fig. 37 for modules ID numbers and visualization of a complete MCORD setup):
 - rectangular modules (length = 4.784 m, width = 0.675 m)
 - detection efficiency $\eta = 0.9$ (not a true value, only assumption for simulations)
 - modules placed at circumference of a diameter 6.623 m cylinder

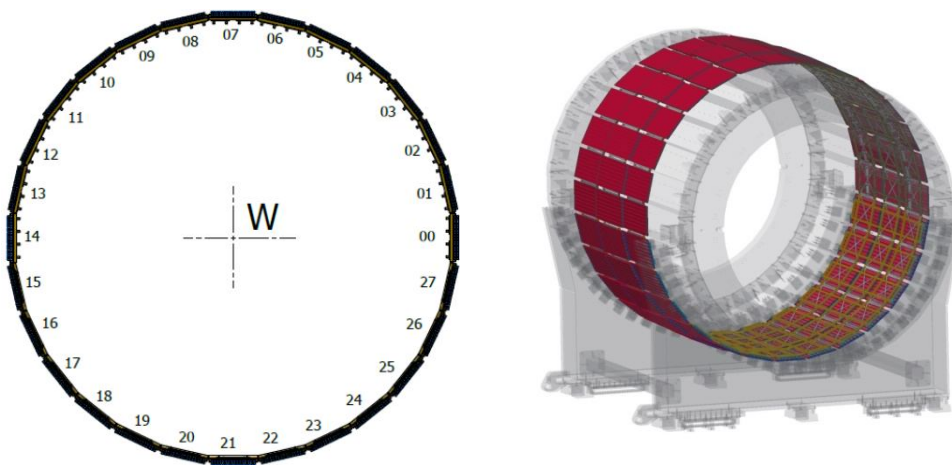


Figure 37 – MCORD sections numbering and visualization of the full setup.

- b. TPC (following TPC CDR, see Figure 38):
 - a single cylinder (length = 3.4 m, radius = 1.1 m)
 - detection efficiency $\eta = 1$ (value adopted from the TPC TDR document)
 - cylinder axis of symmetry at $x = 0, z = 4$

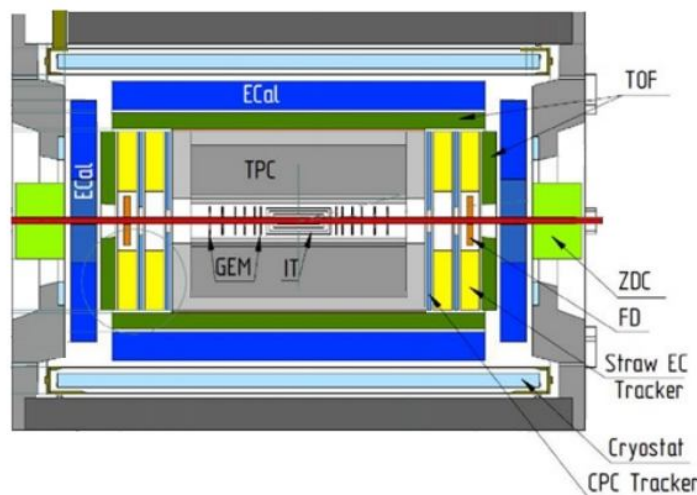


Figure 38 – TPC visualization inside the MPD.

- c. ToF (following ToF CDR, see Figure 39)
 - rectangular modules (length = 5.846 m, width = 0.66 m)
 - detection efficiency $\eta = 0.94$ (value adopted from the ToF TDR document)
 - modules placed at circumference of a diameter 1.5 m cylinder

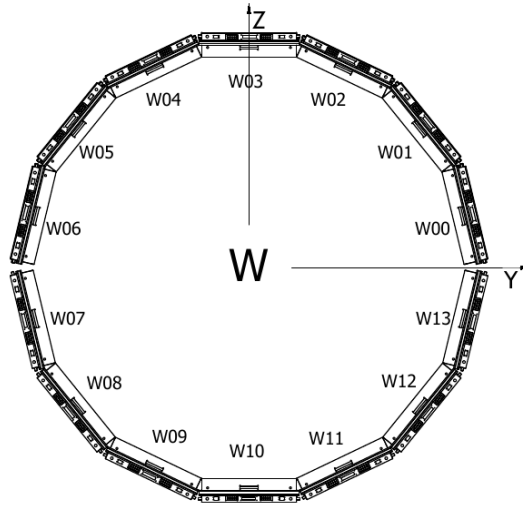


Figure 39 – ToF detectors numbering inside the MPD.

Plotting all points of interaction on the surface of this detector setup reveals its geometry, as shown in Figure 40.

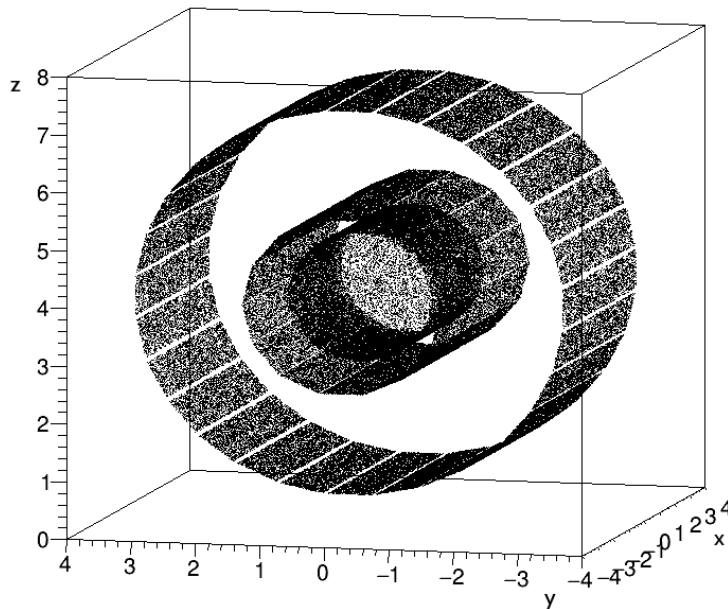


Figure 40 – Plot of all hit positions of the analyzed detector setup.

As a next step, we studied coincidences due to muon counts between MCORD modules set at various locations around the MPD. An example of geometry with 3 modules on the top and 3 modules on the bottom surface of the magnet coil is presented in Fig. 41a. The result shows points of muon interactions in one of the top and bottom detectors that would produce a coincidence signal (Fig. 41b). The distribution of p_{θ} and p_{ϕ} of counted

particles can be plotted (Fig. 41c), so the angular acceptance of the given coincidence can be analyzed.

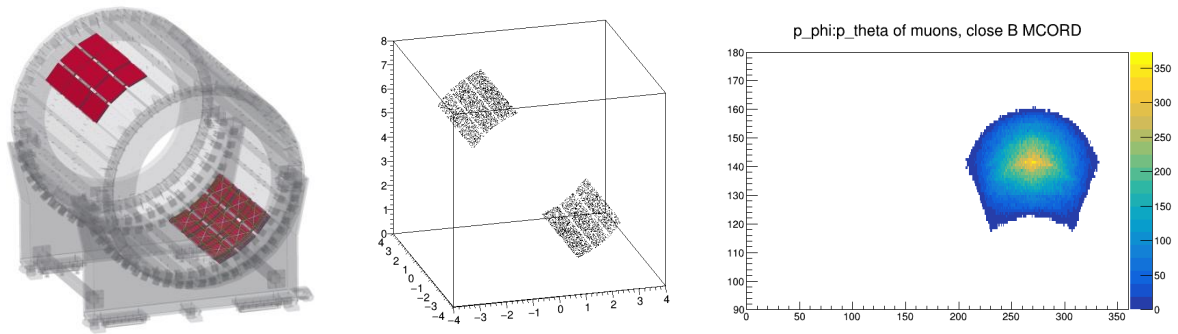


Figure 41 – Coincidence of selected MCORD modules.

41a – position of modules around MPD magnets, 41b – hit positions 3D plot, 41c – angular acceptance of this coincidence.

Subsequently, we investigated the number of events that could be used for TPC calibration. Since the MCORD modules can be reinstalled in different positions around the MPD, we studied the number of coincidence signals per hour for configurations presented in Fig. 42. The number of coincidences per hour between one of the top and one of the bottom modules that produce tracks crossing the TPC are reported in TABLE 6. The numbers are getting lower as expected due to incoming muon flux distribution.

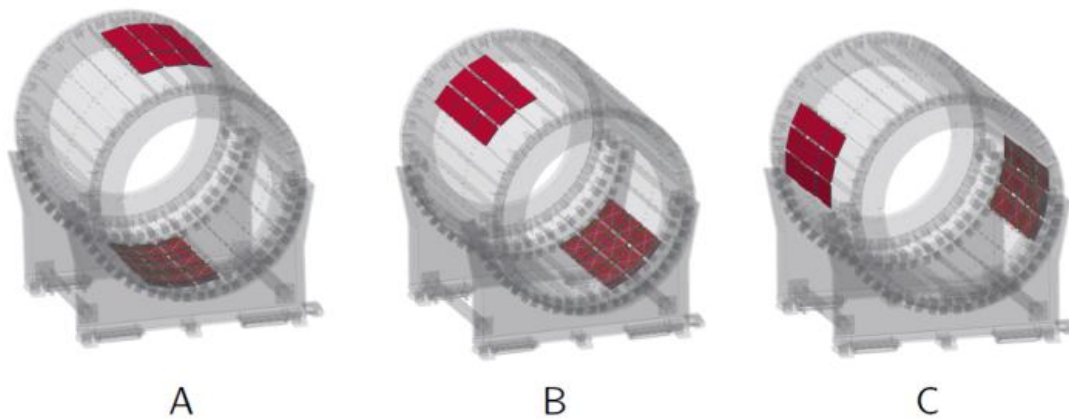


Figure 42 – MCORD configurations A, B and C for TPC calibration.

Table 5 – Number of counts per hour for coincidence events detected by two MCORD modules and TPC calculated for muons with momentum $p > 1.6 \text{ GeV}/c$.

| MCORD configuration | MCORD modules ID numbers | MCORD & TPC (tracks per hour) |
|---------------------|---|-------------------------------|
| A | (6 or 7 or 8) and (20 or 21 or 22) | 246800 |
| B | (9 or 10 or 11) and (23 or 24 or 25) | 158262 |
| C | (12 or 13 or 14) and (26 or 27 or 0) | 20634 |

Fig. 43 shows distribution of track lengths that pass through TPC and give coincidence signals in MCORD modules. The most probable value is equal to the TPC cylinder diameter (2.2 m). Shorter paths appear due to tracks along chords of the TPC, longer paths appear when track crosses or passes near the TPC axis and the MCORD points of interactions are not on the same plane perpendicular to the TPC axis.

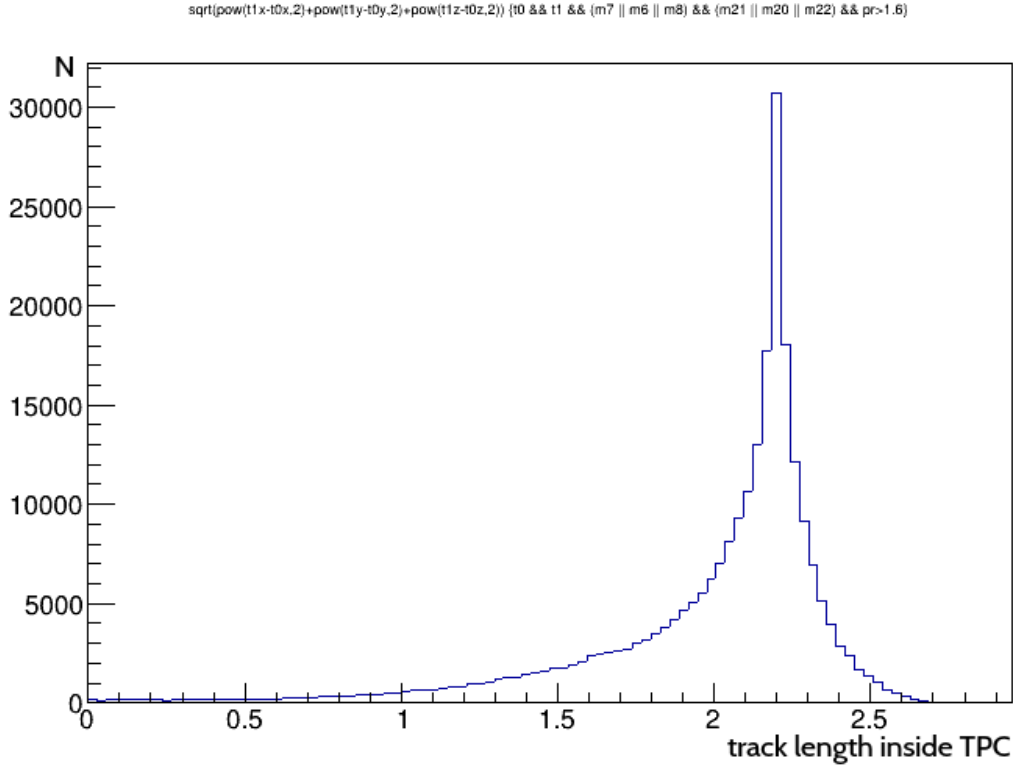


Figure 43 – Distribution of track lengths for coincidence events.
The tracks detected by two MCORD modules and TPC for configurations A, B and C.

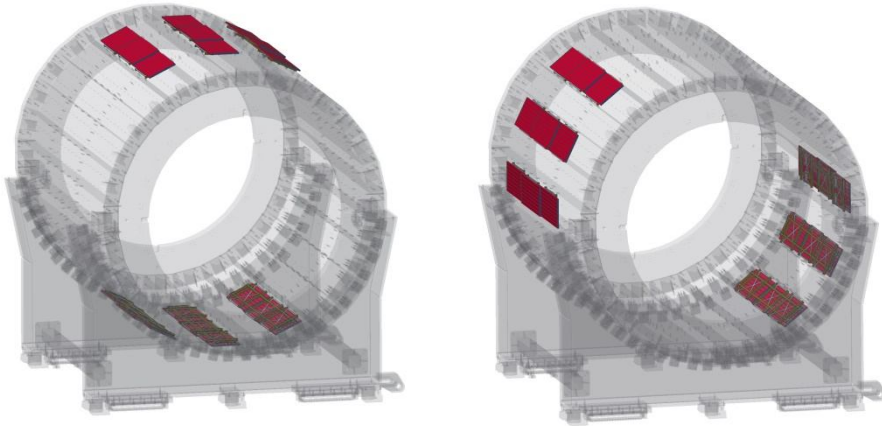


Figure 44 – MCORD configurations D and E for TPC calibration.

The presented approach requires 3 configurations of modules to collect TPC calibration data. Although the system is relatively simple for relocation, it needs some effort and time to collect sufficient amount of data. In order to reduce time necessary for

TPC calibration, we propose to employ two configurations of MCORD modules installed with some gaps between them as presented in Fig. 42. The number of coincidences per hour between one of the top and one of the bottom modules that produce tracks crossing the TPC are reported in TABLE 7.

Table 6 – Number of counts per hour for coincidence events detected by two MCORD modules and TPC calculated for muons with momentum $p > 1.6 \text{ GeV}/c$.

| MCORD configuration | MCORD modules (ID numbers) | MCORD & TPC (tracks per hour) |
|---------------------|---|-------------------------------|
| D | (5 or 7 or 9) and (19 or 21 or 23) | 178822 |
| E | (10 or 12 or 14) and (24 or 26 or 0) | 50894 |

Fig. 45 shows distribution of track lengths that pass through TPC and give coincidence signals in MCORD modules. Gap at 2.1 m appears due to separation of MCORD modules on the surface of the MPD magnet coil.

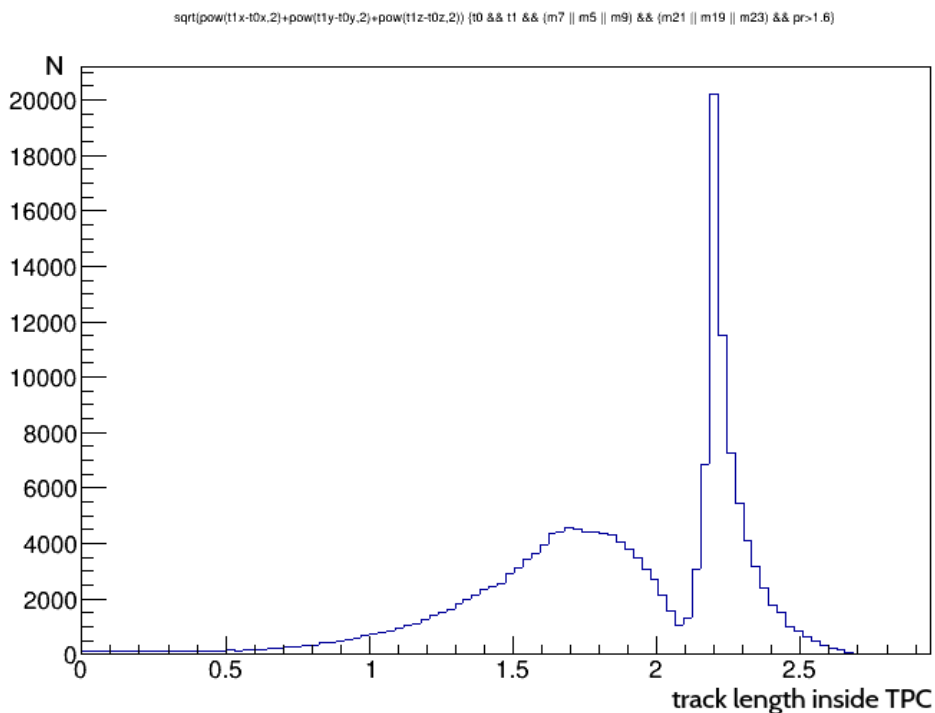


Figure 45 – Distribution of track lengths for coincidence events.

The tracks detected by two MCORD modules and TPC for configurations D and E.

MCORD modules could be used also for ToF calibration after installation inside MPD. Fig. 46 presents relative positioning of MCORD and ToF modules in the MPD. The simulation of muon interactions were performed for several MCORD configurations:

- F: (6 or 7 or 8) and (20 or 21 or 22),
- G: (4 or 5 or 6) and (18 or 19 or 20),
- H: (2 or 3 or 4) and (16 or 17 or 18),
- I: (0 or 1 or 2) and (14 or 15 or 16).

Note that except for MCORD & ToF coincidence events, these configurations provide also tracks that pass the TPC detector, thus it is possible to collect data with MCORD & ToF & TPC coincidences. Tables 8 through 10 provide number of tracks per hour calculated with various muon momentum thresholds: $p > 0.1$ GeV/c (all generated muons), $p > 1.6$ GeV/c (muons able to pass through MPD magnet yoke) and $p > 10$ GeV/c (muons with high enough energy to produce straight tracks across the MPD). In the case of 1.6 GeV/c threshold, the number of tracks that could be used for calibration is reduced by a factor of 2. In the case of 10 GeV/c threshold, the number of tracks that could be recorded for calibration of TPC and ToF drops down to 8% of all tracks observed at $p > 0.1$ GeV/c.

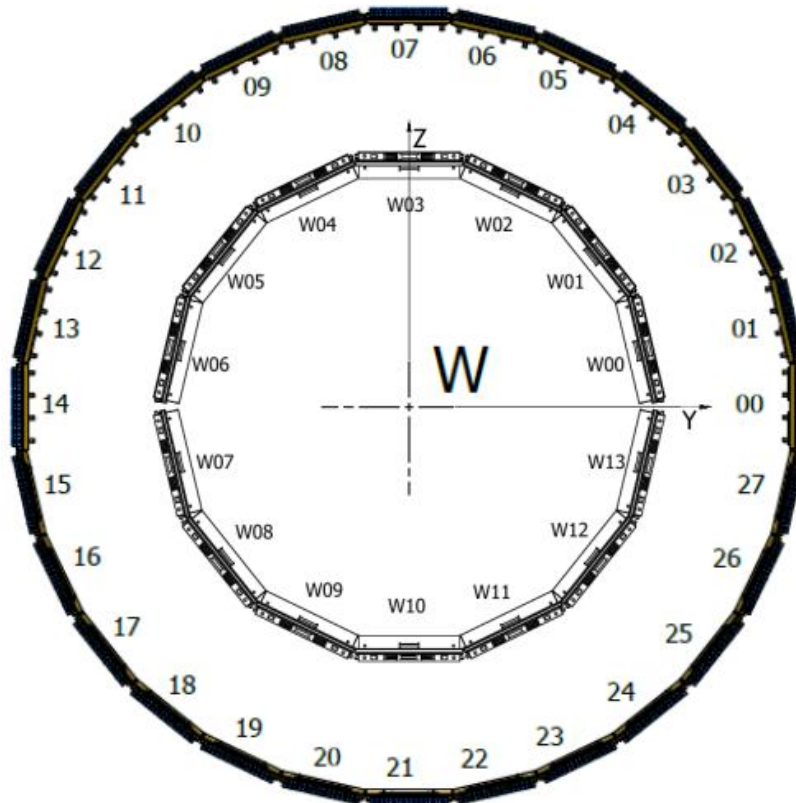


Figure 46 – MCORD (outer ring) and ToF (inner ring) MPD sections numbering.

Table 7 – Number of counts per hour for coincidence events detected by two MCORD modules and ToF or two MCORD modules and ToF and TPC calculated for muons with momentum $p > 0.1$ GeV/c.

| MCORD configuration | MCORD modules (ID numbers) | ToF modules (ID numbers) | MCORD & ToF (tracks per hour) | MCORD & ToF & TPC (tracks per hour) |
|---------------------|------------------------------------|--------------------------|-------------------------------|-------------------------------------|
| F | (6 or 7 or 8) and (20 or 21 or 22) | 3 and 10 | 84558 | 77460 |
| G | (4 or 5 or 6) and (18 or 19 or 20) | 2 and 9 | 68853 | 63792 |
| H | (2 or 3 or 4) and (16 or 17 or 18) | 1 and 8 | 34244 | 31740 |
| I | (0 or 1 or 2) and (14 or 15 or 16) | 0 and 7 | 6136 | 5682 |

Table 8 – Number of counts per hour for coincidence events detected by two MCORD modules and ToF or two MCORD modules and ToF and TPC calculated for muons with momentum $p > 1.6 \text{ GeV}/c$.

| MCORD configuration | MCORD modules (ID numbers) | ToF modules (ID numbers) | MCORD & ToF (tracks per hour) | MCORD & ToF & TPC (tracks per hour) |
|---------------------|------------------------------------|--------------------------|-------------------------------|-------------------------------------|
| F | (6 or 7 or 8) and (20 or 21 or 22) | 3 and 10 | 43493 | 39768 |
| G | (4 or 5 or 6) and (18 or 19 or 20) | 2 and 9 | 35554 | 32958 |
| H | (2 or 3 or 4) and (16 or 17 or 18) | 1 and 8 | 17516 | 16254 |
| I | (0 or 1 or 2) and (14 or 15 or 16) | 0 and 7 | 3143 | 2932 |

Table 9 – Number of counts per hour for coincidence events detected by two MCORD modules and ToF or two MCORD modules and ToF and TPC calculated for muons with momentum $p > 10 \text{ GeV}/c$.

| MCORD configuration | MCORD modules (ID numbers) | ToF modules (ID numbers) | MCORD & ToF (tracks per hour) | MCORD & ToF & TPC (tracks per hour) |
|---------------------|------------------------------------|--------------------------|-------------------------------|-------------------------------------|
| F | (6 or 7 or 8) and (20 or 21 or 22) | 3 and 10 | 6648 | 6069 |
| G | (4 or 5 or 6) and (18 or 19 or 20) | 2 and 9 | 5590 | 5196 |
| H | (2 or 3 or 4) and (16 or 17 or 18) | 1 and 8 | 2713 | 2503 |
| I | (0 or 1 or 2) and (14 or 15 or 16) | 0 and 7 | 480 | 445 |

5.3 Detector Response Simulations

MCORD can be also potentially used as a source of additional data for particle identification in the case of observation of decay products with energy high enough to penetrate the MPD with its yoke. Figure 47 shows the results of simulations of particle propagation through the central volume of the MPD (only particles with $|Z| < 100 \text{ cm}$, where Z direction is parallel to beam axis, were considered). The simulations were based on central (0-5%) Bi-Bi collisions at $\sqrt{s_{NN}} = 9 \text{ GeV}$ generated by the UrQMD 3.4 model. The collisions took place in the center of the detector. Due to limited amount of physical processes implemented in UrQMD model, there were no primary muons in this sample of data. Secondary particles with momentum smaller than $100 \text{ MeV}/c$ were not taken into account in this analysis. The flux of particles is therefore defined by production of primary particles in a collision and:

- interaction of reaction products with the MPD detector (absorption, production of electromagnetic cascades etc.);
- decays of unstable particles;
- particles with $\eta \neq 0$ will eventually leave the central area of MPD.

The example in Figure 47 shows how the relative value of flux decreases after passing through successive layers of MPD. As you can see, the ECal detector, MPD cryostats and yoke have the greatest impact on flux. Vertical lines show the location of the end of individual subsystems. The MCORD detector is proposed to be located at a distance of about 340 cm from the beam line. Only 1% of secondary μ^+ will reach the MCORD detector. Primary and secondary π^+ will be suppressed at MPD outer diameter by a factor of 10^4 and 10^3 , respectively, yielding only 1 particle per 100 collisions.

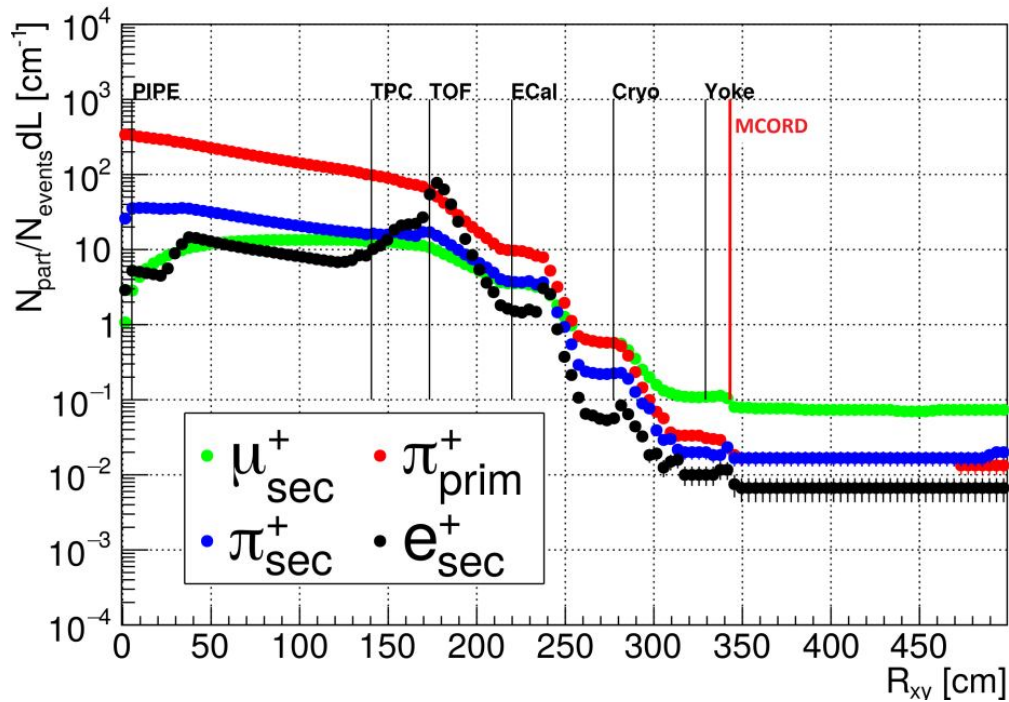


Figure 47 – Muons and pions distribution inside the MPD.

Simulations with UrQMD model shows that approximately 90% of muons are created from pions, approximately 75% of μ^+ and 84% of μ^- come from decays of primary pions. However there is significant difference between production scenario of negatively and positively charged muons created from these particles. We can define two types of pions that decay into muons:

- “moving” pions with $p > 0$, muons produced from these pions are produced mostly in central region of MPD (TPC, beam pipe) where the density of primary pions is the biggest, energy spectrum is similar to the spectrum of pions (exponential-like shape)
- “stationary” pions with $p \approx 0$, muons produced from these particles have $E \approx m_\mu$ (part of energy is carried by ν_μ) therefore we have sharp peak in energy spectrum. Stationary pions are created when “moving” pions are slowed down by the detector, therefore such muons are produced in parts of MPD with high density of material (like ECal or magnet).

Both positive and negative pions decay into a muon and (an) a (anti) neutrino pairs, however, once slowed down, only π^+ are source of secondary μ^+ , as π^- bind with nuclei in the surrounding matter and does not contribute to secondary μ^- yield. The difference in the secondary muon yields with respect to their charge is presented in Fig. 48. The left plots show the creation points of positive and negative muons in the MPD, the right plots shows

points of creation of only those muons, that could be registered with MCORD. The usefulness of MCORD for tracing these asymmetries will be subject for future studies. Possibility of using MCORD data for identification of rare meson decays through dilepton channels will also be investigated.

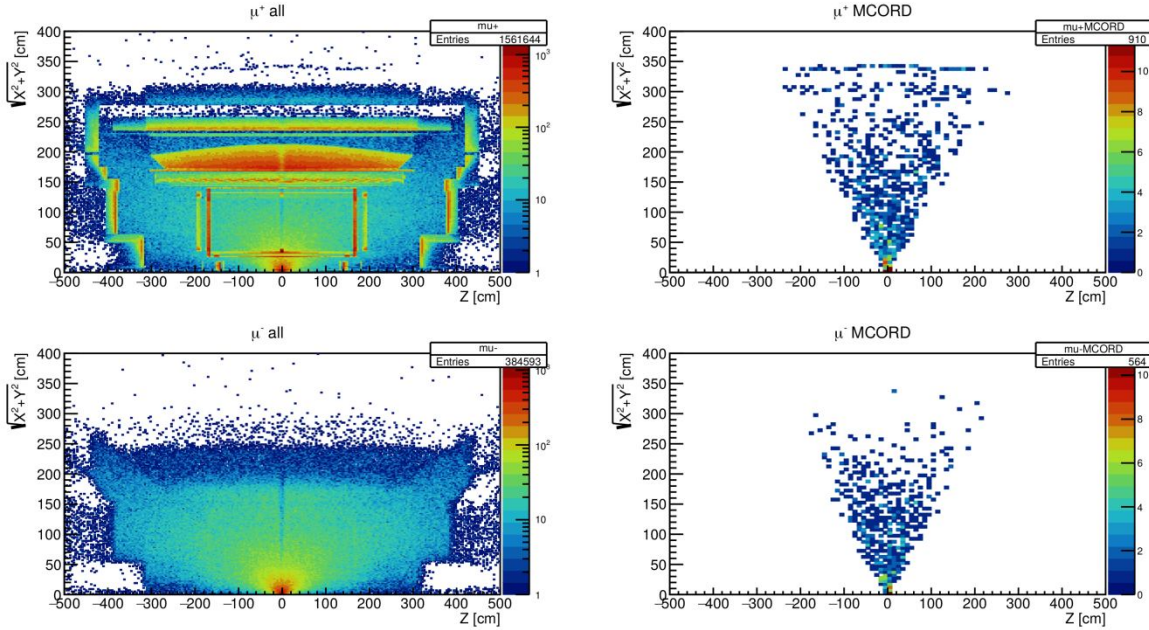


Figure 48 – The points of creation of negative and positive muons.

Top plots corresponds to μ^+ whereas μ^- are at the bottom. Left plots represents points of creations any muon whereas right plots shows points of creations muons that can be detected by MCORD. The structure of detector (contribution from decays of “stationary” particles) is clearly visible for positive muons.

5.4 Detector Performance Evaluation

First laboratory tests of plastic scintillators lined with one WLS fiber were done with plastic bar size $1500 \times 72 \times 22 \text{ mm}^3$, also delivered by NUVIA Company. The results of dark counts and muon response were recorded using a CAEN digitizer 57308B in both single and coincidence modes. Coincidence measurements were done with two plastic hodoscopes coupled to photomultiplier tubes (PMTs). The size of the hodoscopes was $50 \times 50 \times 50 \text{ mm}^3$.

As a first test of the laboratory characterization procedure, the dark counts spectra measured for the SiPMs coupled to WLS fibers were recorded in single acquisition mode. An exemplary spectrum is presented in Figure 49. Marked peaks are related with detector response to 1, 2, 3 etc. pixels fired. The mean distance between those peaks gives the amplitude of signal from one pixel excited by one photon absorbed. In standard operation the recorded signals are a sum of pulses from pixels excited by absorbed photons. In the presented case, the amplitude of the signal from 1 pixel is equal to 74 channels. Since one pixel is fired by one photon, and SiPM operation has some analogy with the PMT operation, it is common to use term “photoelectron” (phe) to report amplitudes of the recorded signals.

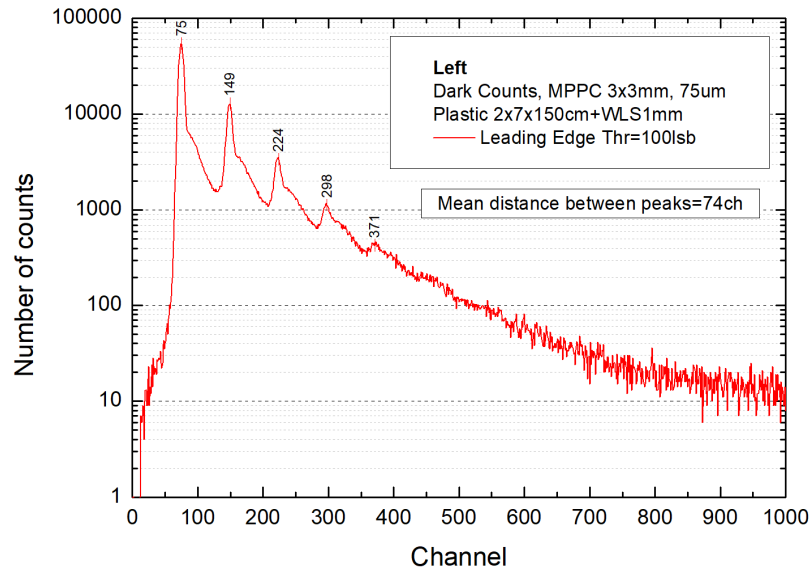


Figure 49 – The energy spectra of dark counts.

Recorded with $3 \times 3 \text{ mm}^2$ MPPC photodetector coupled to 1mm diameter WLS fiber placed at one end of $1500 \times 72 \times 22 \text{ mm}^3$ plastic slab.

Once this simple characteristics of the SiPMs placed on both ends of the plastic bar were quantified, we measured the amplitudes of signals induced by muons passing through the detector. The measurements were carried out using signals from the plastic hodoscopes placed above and under the tested detector to provide a trigger gate for the acquisition setup (Figure 50). The trigger gate was adjusted to enable acquisition only if a muon passes through both hodoscopes, in this way the interaction point was limited to the area determined by the size of the hodoscopes cross section, i.e. $5 \text{ cm} \times 5 \text{ cm}$ square. The energy spectra of the muons detected in the plastic are formed by pulses of tens of photoelectrons and show slight dependence on the interaction point (Figure 51), i.e. the amplitude decreases as the distance between the muon interaction point and the SiPM increases. Please notethat the energy spectra of muons were binned 4 times in comparison to dark counts response and the dark count response was measured at 4 times higher gain then muon response. As a result, the scaling factor for the dark count spectra is $\times 16$ in comparison to muon response.

The response of the scintillator bar to muons was also simulated using GEANT4 code. A perpendicular muon flux impinging $5 \times 5 \text{ cm}^2$ surface of the detector was considered at the same distance from the end as during laboratory measurements. The results of the simulations are in very good agreement with experimental data (Figure 51).

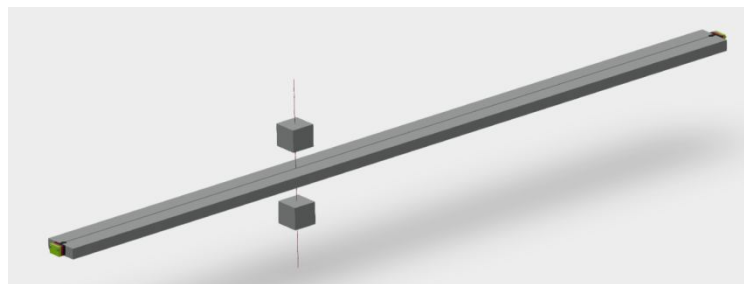


Figure 50 – The experimental setup for measuring the coincidence.

Coincidence resolving time of muons recorded in a double-sided MPPC readout from a plastic slab with a WLS fiber

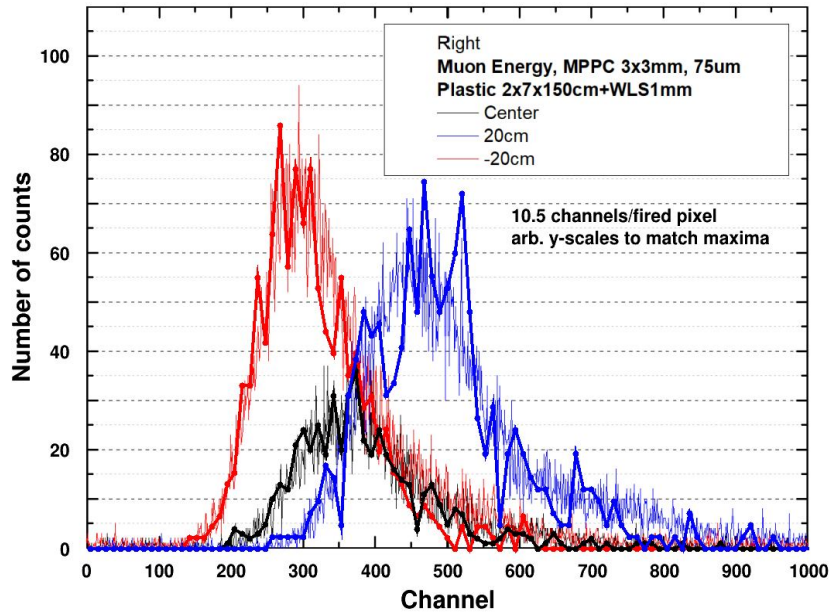


Figure 51 – The muons energy spectra.

Energy spectra recorded in the center, -20 cm and +20cm position along the plastic slab plastic slab (thin lines). Results of simulations assuming the same experimental conditions are presented with thick lines.

In order to measure the position of muon interaction along the plastic bar, the difference in arrival time of signals (i.e. Coincidence Resolving Time – CRT) reaching both ends of the scintillator was recorded. Figure 52 presents the distributions measured for different positions of the hodoscopes along the plastic bar. The coincidence time T_{diff} distribution measured in the center of the bar is plotted in black, pairs of distributions marked with other colors show results of measurements done at the same distance to the left and to the right from the center. The values shown in the middle of the distributions show full width at half maximum values. The standard deviation σ_T is then given by $FWHM_T$ as follows:

$$\sigma_T = FWHM_T / 2.355 \quad (1)$$

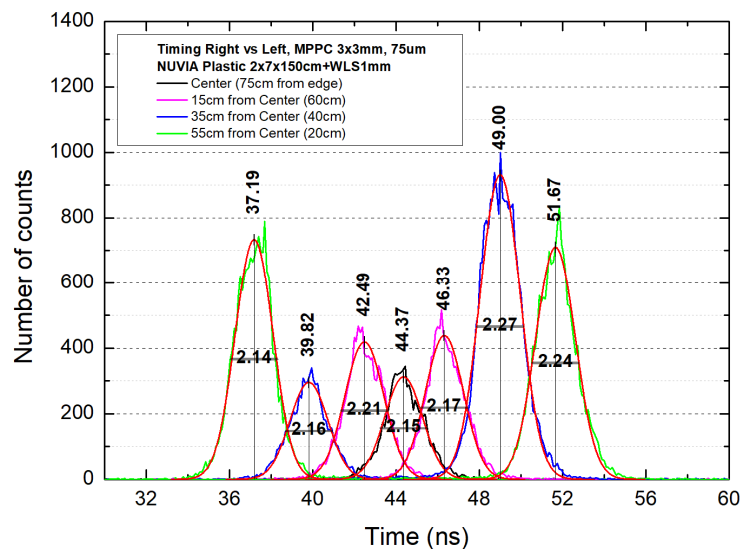


Figure 52 – Timing spectra recorded for muons.

Spectra recorded in $1500 \times 72 \times 22 \text{ mm}^3$ plastic slab with 1 mm WLS fiber and double-sided $3 \times 3 \text{ mm}^2$ SiPM light readout.

Figure 53 presents a plot of the distance between the muon interaction point defined by the hodoscopes and one of the sides as a function of measured time difference T_{diff} reveals a linear dependence given by a formula:

$$x = (c'/2) \times T_{diff} + const \quad (2)$$

where c' denotes the speed of light in the detector. Fitting a line to the data allows calculating this value, which amounts to 15.22 cm/ns in our case.

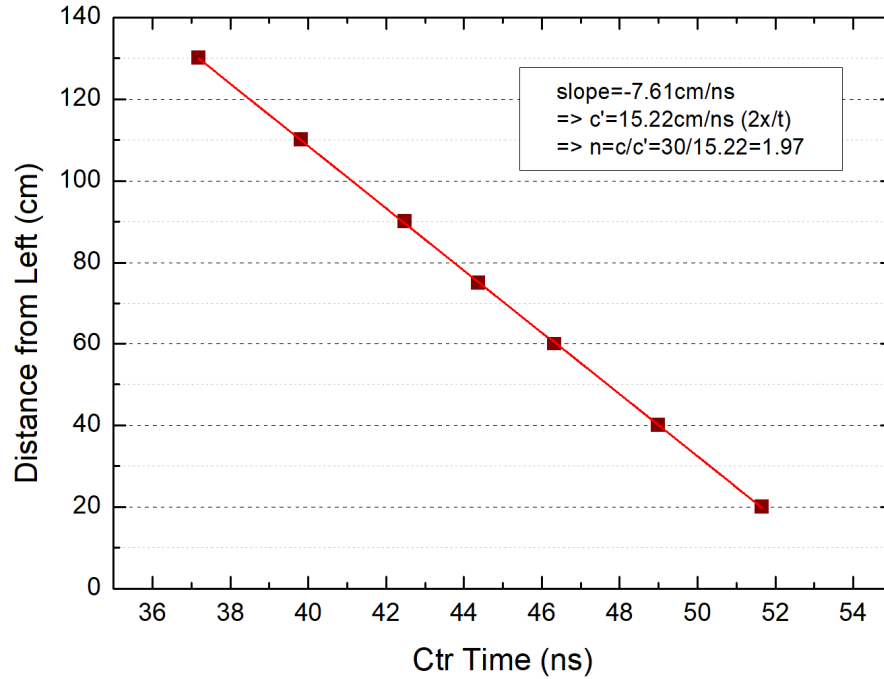


Figure 53 – The relation between the CRT time and the distance.

The distance between the interaction point and left side of the plastic slab.

Having this result, we can now calculate the uncertainty of the interaction position along the scintillator bar using a formula:

$$\Delta x = c'/2 \times \Delta T_{diff} \quad (3)$$

Thus, $FWHM_T$ equal to 2.19 ns as seen in Figure 41 that corresponds to $\sigma_T = 0.93$ ns results in the positional accuracy (σ_x) of 7.1 cm. Broadening of interaction position distribution due to finite size of our hodoscopes (5×5 cm²) was found negligible.

In parallel with the assembly of 16 scintillator bars for two MCORD demonstrator sections, R&D activities are carried on. The results of laboratory tests show that application of a 2 mm diameter WLS fiber instead of the currently used 1 mm diameter fiber improves the time resolution to 0.80 ns, whereas installation of two 1 mm diameter WLS fibers in one bar with separate light readout devices allows to achieve $\sigma_T = 0.73$ ns.

6 References

- [1] Ref.: <http://nica.jinr.ru/complex.php>
- [2] V. Golovatyuk, V. Kekelidze, V. Kolesnikov, O. Rogachevsky and A. Sorin, The Multi-Purpose Detector (MPD) of the collider experiment, *Eur. Phys. J. A* (2016) 52: 212
- [3] D. Dabrowski et al., Gas System for MPD Time-of-Flight Detector, *Act.Phys.Pol.B* Vol.92 No.2 p.203 (2016)
- [4] K. Roslon et al., The Cooling, the Regulation and the Temperature Stabilization System for MPD Detector at JINR Accelerator Complex NICA, *Act.Phys.Pol.B* Vol.92 No.2 p.299 (2016)
- [5] http://mpd.jinr.ru/wp-content/uploads/2019/10/TDR_NICA-MPD-PLATFORM_EN_190520.pdf
- [6] T. Stanev, High Energy Cosmic Rays, Springer-Praxis book, (2009)
- [7] M. Bielewicz et al., MCORD: MPD cosmic ray detector for NICA, *Proc. SPIE* Vol. 10808 No. 1080847 (2018)
- [8] M. Bielewicz et al., MCORD - MPD Cosmic Ray Detector a new features, *EPJ Web Conf.* Vol. 204 No 07016 (2019)
- [9] A. Fernández et al., ACORDE a cosmic ray detector for ALICE, *Nucl. Instrum. Methods Phys. Res., A* 572 (2007) p.102-103
- [10] M. Grodzicka-Kobylka, T. Szczesniak, M. Moszynski, Comparison of SensL and Hamamatsu 4x4 channel SiPM arrays in gamma spectrometry with scintillators, *Nucl. Instrum. and Meth. in Phys. Res. A*, Vol. 856, p.53 (2017)
- [11] <https://www.picmg.org/openstandards/microtca/>
- [12] <http://mpd.jinr.ru/wp-content/uploads/2019/01/TpcTdr-v07.pdf>
- [13] http://mpd.jinr.ru/wp-content/uploads/2019/01/TDR_TOF_MPD_v3_0-08_11_2018.docx
- [14] <https://eljentechnology.com/products/plastic-scintillators/ej-200-ej-204-ej-208-ej-212>
- [15] <https://www.crystals.saint-gobain.com/products/bc-408-bc-412-bc-416>
- [16] <https://www.ni.com/pl-pl/innovations/white-papers/06/controller-area-network--can-overview.html>
- [17] <https://www.ohwr.org/projects/wr-std/wiki>
- [18] W.M. Zabolotny, A. Byszuk, Algorithm and implementation of muon trigger and data transmission system for barrel-endcap overlap region of the CMS detector, *Journal of Instrumentation*, Vol. 11, p. C03004 (2016)
- [19] U Bhawandeep et al., The CMS trigger system, *Journal of Instrumentation*, Vol. 12, pp. 1-122 (2017)
- [20] W.M. Zabolotny et al., Implementation of the data acquisition system for the Overlap Muon Track Finder in the CMS experiment, *Journal of Instrumentation*, Vol. 12, p. C01050 (2017)

- [21] M. J. Peryt, T. Traczyk, EqDb – Equipment Database for Complex Experiments, Act.Phys.Pol.B Vol.92 No.2 p.293 (2016)
- [22] CORSIKA: a Monte Carlo code to simulate extensive air showers., by Heck, D.; Knapp, J.; Capdevielle, J. N.; Schatz, G.; Thouw, T., Forschungszentrum Karlsruhe GmbH, Karlsruhe (Germany)., Feb 1998, V + 90 p., TIB Hannover, D-30167 Hannover (Germany).
- [23] S.Agostinelli et al., Geant4—a simulation toolkit, Nuclear Instruments and Methods in Physics Research, A 506 (2003) 250-303
- [24] C.J. Werner, J.S. Bull, C.J. Solomon, et al., "MCNP6.2 Release Notes", LA-UR-18-20808 (2018).
- [25] ALICE Collab., Study of cosmic ray events with high muon multiplicity using the ALICE detector at the CERN Large Hadron Collider, JCAP 01 (2016) 032
- [26] J. Abdallah et al., DELPHI Collab., Study of multi-muon bundles in cosmic ray showers detected with the DELPHI detector at LEP, Astroparticle Physics 28 (2007) 273
- [27] V. Avati et al., Cosmic multi-muons events observed in the underground CERN-LEP tunnel with the ALEPH Experiment, Astroparticle Physics 19 (2003) 513
- [28] I. Yashin et al., Investigation of Muon Bundles in Horizontal Cosmic, ICRC 28 (2005) p.1147-1150
- [29] V. Berezhinsky, M. Kachelrieß, and A. Vilenkin, Ultrahigh Energy Cosmic Rays without Greisen-Zatsepin-Kuzmin Cutoff, Phys. Rev. Lett. 79, (1997) 4302
- [30] P. Kankiewicz, M. Rybczynski, Z. Wlodarczyk, G. Wilk, Muon Bundles as a Sign of Strangelets from the Universe, Astrophysical Jour., Vol.839 (2017) p.31
- [31] M. Tanabashi et al. (Particle Data Group), Review of Particle Physics, Phys. Rev. D 98 (2018) 030001.
- [32] P. Shukla, S. Sankrith: Energy and angular distributions of atmospheric muons at the Earth. <https://arxiv.org/pdf/1606.06907.pdf>
- [33] Cosmic Ray Division: <http://crd.yerphi.am/Muons>